Eur. Phys. J. A (2023) 59:102
https://doi.org/10.1140/epja/s10050-023-00978-w

THE EUROPEAN PHYSICAL JOURNAL A

Regular Article - Experimental Physics

# Radioactive decays of stored highly charged ions

**Yury A. Litvinov**[a], **Rui Jiu Chen**[b]

Atomic, Quantum & Fundamental Physics Division, GSI Helmholtz Center for Heavy Ion Research GmbH, Planckstraße 1, Darmstadt 64291, Hesse, Germany

Received: 22 January 2023 / Accepted: 10 March 2023 / Published online: 10 May 2023

Communicated by Nicolas Alamanos

**Abstract** Decay properties known in neutral atoms can be altered significantly if all or most bound electrons are removed. Straightforwardly, in fully-ionised nuclei, the decay channels involving electrons are simply disabled. Also decay modes, that are hindered or completely blocked in neutral atoms, may, respectively, become dominant or open up in highly charged ions. Few-electron ions are by themselves clean systems with well-defined quantum numbers, in which the interactions within the remaining electrons can either be excluded or treated precisely, thereby allowing for investigations of the influence of atomic shell on nuclear decay properties. Violent stellar environments characterised by high temperatures and densities lead to high ionisation degrees of nuclides involved in nucleosynthesis processes. In spite of the rich motivation for studying radioactive decays of highly charged ions, intensive measurements became possible only after heavy-ion storage rings coupled to radioactive-ion beam facilities became available. Presented here is a compact review of the relevant experimental techniques and experiments.

## 1 Introduction

The discussion on whether decay rate of a nucleus is its fundamental constant or it can be manipulated by external means goes back to the beginning of the last century, when the discovery of radioactivity went hand-in-hand with the first attempts to alter its properties [1–3]. The motivations for finding ways to change nuclear rates are manyfold. Indeed, if such alchemy was possible, the impact on our daily life would be immense. One could then dream about production and enrichment of low-abundance elements or about changing waste composition, as well as about many other applications in astronomy, geology, biology, medicine, chemistry, etc.

However, in numerous experiments on atoms, aiming at modifying nuclear decay probabilities by varying temperature, pressure, electric and magnetic fields, chemical environments, acceleration and other parameters, only tiny modifications of below about 1% were observed, which were attributed to changes of the electron density at the nucleus.

A perturbation of the orbital electron capture (EC) rate by implanting atoms in different media was addressed by Segrè in 1947 [4]. This has independently been suggested also by Daudel [5], who in addition indicated that internal conversion (IC) de-excitation of nuclear isomeric states can as well be affected. Soon after, Segré and Wiegand found small changes in the EC probability of $^{7}$Be by comparing its half-life in a pure metal sample and in BeO or $BeF_2$ compounds [6]. In this context, $^{7}$Be is probably the most intensively studied case, see e.g. [7–11]. Apart from basic understanding of radioactivity, it is valuable for solar physics, where the EC decay of $^{7}$Be, ionised in solar plasmas [12,13], affects the electron neutrino flux [14,15].

A huge number of implantation experiments have been conducted to date. Although light atoms are the best-suited probes, effects were also found in heavy atoms up to $^{235m}$U [16]. It is impossible to mention here all studies accomplished. The interested reader is referred to reviews [17,18] and references cited therein.

It is clear that the largest modifications of electron densities are achieved in highly charged ions (HCI). This is obviously true for fully-ionised atoms, where the electron density at the nucleus is just zero and all decays involving bound electrons are disabled. Extensive systematic studies of decays of HCIs became possible in the 1990 s with the advent of heavy-ion storage rings coupled to radioactive-ion beam facilities [19]. We note that exciting plans exist for measuring radioactive decays of HCIs in electron-ion beam traps

[a] e-mail: y.litvinov@gsi.de (corresponding author)
[b] e-mail: r.chen@gsi.de

(EBIT) [20–22]. First results on charge-bred $^{124}$In and $^{124}$Cs were reported [23].

Stellar nucleosynthesis is one of the major motivations for decay studies of HCIs. It proceeds in environments characterised by huge densities and temperatures [24,25]. Beta decay ($\beta$-decay) alters the proton number and thus plays a decisive role in all nucleosynthesis processes [26–28]. The main routes, responsible for the synthesis of about 99% of chemical elements heavier than iron, are the slow ($s$) and rapid ($r$) neutron capture processes. The respective thermal energies at the corresponding sites reach several keV to about hundred keV. In such violent conditions, involved nuclei are highly ionised and their decay properties can differ from the ones established in neutral atoms [29–32].

Another important motivation is to understand the coupling of the atomic and nuclear degrees of freedom [33–36]. Here, the HCIs offer the possibility to investigate decays of systems with involved leptons being in a well-defined quantum-mechanical state. For example, the parent nuclides can be prepared as bare, hydrogen- (H-like), helium- (He-like), or lithium-like (Li-like) ions. In this way, the complicated interactions of the many bound electrons in atoms, like partial screening of the nuclear charge by the electron cloud, can be treated exactly in few-electron systems [37].

In this work, we review experimental results on the radioactive decays of HCIs obtained at heavy-ion storage rings to date and give an outlook on future research. In 2011, a compilation of then available results has been published in [38]. It is updated here.

## 2 Beams of highly charged radioactive ions

The prerequisite for decay studies of radioactive HCIs is their production in a nuclear reaction and in a (high) atomic charge state of interest, separation from inevitable contaminants, and injection and storage in an ultra-high vacuum environment of a storage ring [39].

There are two complementary methods to produce radioactive ions in high atomic charge states. One of them is the *Isotope Separation On-Line* (ISOL), which delivers, except for some chemical elements, intense beams of low charged (typically $q = 1+$) radioactive ions [42]. Thick targets are utilised, in which high-energy light projectiles lead to creation of short-lived nuclei through target spallation or fission nuclear reactions [43]. Diffused to an ion source particles are extracted at low energies. The ISOL beams have small emittances and are thus well suited for charge breeding in an *Electron Beam Ion Source/Trap* (EBIS/T) [44–46]. The resulting HCIs have low kinetic energies ideal for their subsequent incarceration in an ion trap [47–49]. The overall HCI production chain can be as fast as a few tens of milliseconds. This is the basic procedure utilised for decay spectroscopy

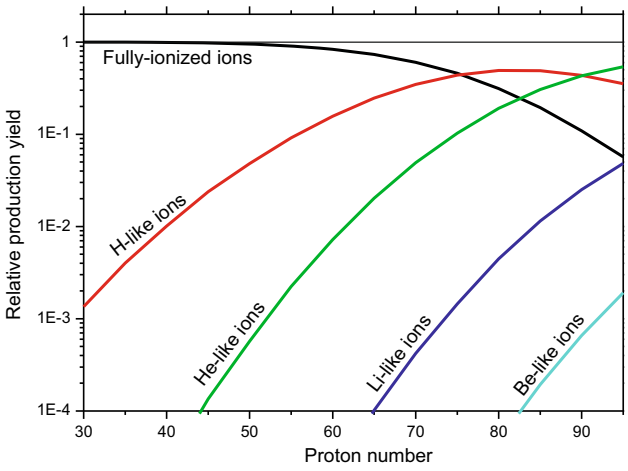


**Fig. 1** Calculated with the GLOBAL code equilibrium charge state distributions of different projectiles emerging the $^{9}$Be metal foil at 400 AMeV exit energy [40]. The figure is adopted from [41]

in traps mentioned in Sect. 1 as well as in low-energy storage rings, which are being considered at ISOL facilities, see Sect. 7.

Another approach is the *in-flight* production and separation of exotic nuclei. This method is presently employed at all operating heavy-ion storage ring facilities, that are discussed in Sect. 3. All of them are coupled to in-flight fragment separators [50,51]. Different nuclear reactions can be utilised for production of radioactive nuclei in various regions of the nuclidic chart. In our context, fragmentation of relativistic heavy primary beams and fission of uranium beams on thin targets of light elements are the most commonly used nuclear reactions [43,52]. Projectiles at relativistic energies of about 100–600 MeV/u are typically employed.

HCIs are produced through stripping of bound electrons by sending energetic fragments through matter [40,52,53]. Here, the production target is simultaneously used for the electron stripping. Calculated equilibrium charge state fractions, the ones independent from the initial charge state of the projectile entering the matter, as a function of proton number ($Z$) are plotted in Fig. 1 for fragments leaving $^{9}$Be target at 400 AMeV energy. By choosing a proper stripper material as well as its thickness, one may enhance population of a specific charge state [54–57].

Distinct from the ISOL beams, the in-flight ones have broad momentum distributions of a few percent [52,58,59]. The fragments are transported by a fragment separator, typically an achromatic device [60], from the target to the experiment, which in our case is the injection into a storage ring. The separator has planes with large dispersion, which are used for magnetic rigidity $B\rho = mv\gamma/q$ analysis. Here $B$ is the magnetic flux density, $\rho$ bending radius, and $m, v, q$, and $\gamma$ are the mass, velocity, charge, and relativistic Lorentz factor of the ion, respectively. The high kinetic energies of the fragments

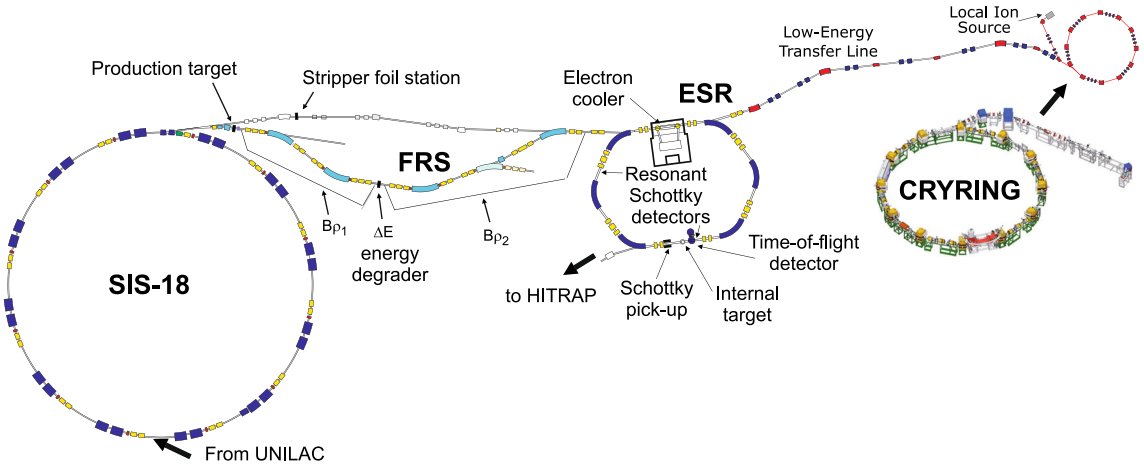


**Fig. 2** Schematic illustration of the secondary-ion beam facility at GSI. The heavy-ion synchrotron SIS receives beams from the linear accelerator UNILAC. Secondary ions are produced either in the production target in front of the in-flight fragment separator FRS or in the direct transfer line in the stripper-foil station. Two stages of magnetic rigidity analysis and energy loss degrader positions in the FRS are indicated. The main components in the storage ring ESR, including the extraction towards HITRAP, are labeled. Shown also is the location of the recently installed low-energy storage ring CRYRING@ESR with its local ion source and injection line. The figure is updated from [64]

allow for adding special solid degraders [60,61]. Since the energy loss ($\Delta E$) is charge dependent, the $B\rho - \Delta E - B\rho$ analysis enables high purification power, such that mono-isotopic beams can be prepared. It is also possible to use different charge states in the first and second $B\rho$ stages and the degrader for changing the charge state distribution in between [62,63].

## 3 Heavy-ion storage ring facilities

There are three heavy-ion storage ring facilities in operation today [51,64].

*The radioactive ion beam facility at GSI* in Darmstadt is a combination of the high-energy heavy-ion synchrotron SIS [65], the in-flight fragment separator FRS [61], and the cooler-storage ring ESR [66]. Except for poisonous source materials like Be, Cd, Tl etc, intense beams of any (semi-)stable nuclide from protons up to uranium can be accelerated by the SIS to the maximum magnetic rigidity $B\rho = 18$ Tm. The ESR can vary the energy of the stored beam within $3\,\text{Tm} \leq B\rho \leq 10\,\text{Tm}$. Decelerated beams can either be ejected towards a dedicated low-energy storage ring CRYRING@ESR, which has recently been commissioned [67,68], or towards the trapping facility, HITRAP [69]. The GSI facility is schematically illustrated in Fig. 2.

The flight time of secondary beams from the target through the FRS until the exit of the separator is a few hundred nanoseconds. This sets the minimal lifetimes of nuclei that can be addressed in the ESR, where the time required for the measurement itself needs to be considered in addition. By employing only the $B\rho$ analysis, cocktail beams can efficiently be transmitted to the ESR, which is frequently used for broadband mass measurements [59]. The $B\rho - \Delta E - B\rho$ separation is used to prepare mono-isotopic beams either for lifetime spectroscopy discussed here or for the in-ring reaction studies [70–75]. In addition, radioactive HCIs can be produced in the direct SIS-ESR beam-line bypassing the FRS [76–78], which is often overbooked with non-ring experiments.

The concept of the *Heavy Ion Research Facility in Lanzhou* (HIRFL) [79,80] is very similar to the one of GSI. The core of the high energy part of HIRFL is the main cooler-storage ring CSRm, which functions as a heavy-ion synchrotron with a maximum $B\rho = 11\,\text{Tm}$. The fragment separator, the second radioactive ion beam line in Lanzhou, RIBLL2, operates as a pure $B\rho$ analyser to transmit cocktail beams of radionuclides to the experimental cooler-storage ring CSRe [81]. The CSRe has a maximum magnetic rigidity $B\rho = 8.4\,\text{Tm}$. The present accelerator chain allows efficient acceleration of beams up to about xenon, which limits the range of secondary systems to be studied. The situation will dramatically improve with the installation of a new linear accelerator as a primary injector of the CSRm [82].

Of utmost importance for lifetime measurements in storage rings is the ability to cool hot secondary beams [83]. Three cooling methods are utilised in storage rings. The electron [84] and stochastic [85] methods are applicable to any types of stored ions and are routinely used [86–89]. A significant progress has been achieved in laser cooling, though it can only be utilised for a limited number of ions [90–92]. Moreover, beam cooling facilitates broad and rapidly developing research programs in atomic and nuclear physics. These can-

not be covered here and the reader is referred to reviews [93–103] and references cited therein.

The driver accelerators at GSI and HIRFL are synchrotrons, which are pulsed machines. Therefore, the beam transmission chain to the storage ring is a synchronised bunch-to-bunch procedure. The facility at *RIKEN Nishina Center for Accelerator-Based Science* is built on a very different principle. The storage ring, Rare-RI Ring (R3) [104], is basically a weak focusing synchrotron. It is composed only of dipole magnets and is run solely in isochronous optics at a fixed rigidity of 5.5 Tm, see Sect. 4.1. The driver accelerator is a superconducting cyclotron, which as of today delivers the most intense primary beams worldwide and as a consequence gives access to the most exotic nuclides. It is therefore attractive to store them in a ring. However, due to the (quasi-)DC characteristics of the cyclotron beams, the injection and investigation of only individual particles one by one is possible [105–107]. Apart from the highest intensities, the strongest advantage of the setup is that each particle is identified within the large-acceptance BigRIPS fragment separator [108] and only the ones of interest generate a valid trigger for the injection into the R3 [109]. No cooling is presently available. Although lifetime measurements of HCIs were not attempted yet, non-destructive diagnostic is being developed [110,111], see Sect. 4.1, which will enable such research in the future.

## 4 Time-resolved storage ring mass spectrometry

The measurements of nuclear decays rely on the *storage ring mass spectrometry* (SRMS). Its basic principle lies in the fact that the mass-over-charge ratio $(m/q)$ of a particle changes in the decay, which can be detected through time-resolved and intensity-resoved SRMS. In the following, we briefly discuss the basics of the SRMS.

### 4.1 Conventional storage ring mass spectrometry

In first-order approximation, the relative revolution frequency deviation $\Delta f/f$ of the stored ions can be related to the relative difference $\Delta(m/q)/(m/q)$ and the velocity spread $\Delta v/v$ via the following expression [115–118]:

$$\frac{\Delta f}{f} = -\frac{1}{\gamma_t^2}\frac{\Delta(m/q)}{(m/q)} + \left(1 - \frac{\gamma^2}{\gamma_t^2}\right)\frac{\Delta v}{v}, \tag{1}$$

where $\gamma$ is the relativistic Lorentz factor and $\gamma_t$ the machine parameter termed *transition energy*. The latter quantity is connected to the momentum compaction factor $\alpha_p$ as $\alpha_p = 1/\gamma_t^2$, which describes the relative change of the orbit length caused by a relative change of magnetic rigidity. $\alpha_p$ is supposed to be constant for a given ion-optical setting of the ring [119,120].

According to Eq. (1), the revolution frequency is the measure of the particle mass-over-charge ratio if the second term on the right-hand side is made negligible. However, the velocity spread of secondary particles produced in a nuclear reaction is huge and is typically larger than the acceptance of the transport beam lines and the injection into the storage ring.

In the conventional *Schottky mass spectrometry* (SMS) [121], the velocity spread of the stored ions is reduced by stochastic and/or electron cooling [122], reaching–for particle intensities of below about 1000 ions–values as small as $\approx 10^{-7}$ [123]. Thus the second term in Eq. (1) can be neglected.

Nuclides with lifetimes exceeding the cooling process, which takes at least several seconds, can be addressed by the conventional SMS.

The revolution frequencies are then measured by non-destructive Schottky diagnostics. The development of Schottky detectors in the ESR is illustrated in Fig. 3. A relativistic particle revolves in a storage ring with a high frequency of a few hundred kHz to a few MHz. Being charged, it periodically induces an electric current on the electrodes of a Schottky detector. The output of the detector, which is dominated by thermal noise, is Fourier analysed, which makes repeating signals visible. The obtained power spectrum contains frequency peaks ordered according to $m/q$ values of the stored ions, see Eq. (1). This is routinely used for precision mass measurements [124–130], where the spectrum is calibrated by the unavoidably present nuclei with well-known masses. Furthermore, the area of a frequency peak is directly proportional to the number of stored particles. By tracing the evolution of peak areas, the corresponding half-lives can be determined. This is the basis of the time-resolved SMS [131].

The first generation of the ESR Schottky detector is illustrated in the left panel of Fig. 3. A sum signal from a pair of oppositely placed capacitive copper plates is typically used [112]. A single stored ion with charge $q > 30$ can be detected within about 30 s. The simultaneously measured bandwidth covers the entire ESR acceptance [126]. An example of the measured decays in the ESR is shown in Fig. 4.

The need for a faster detector led to a development of a pill-box cavity resonator [113], see the middle panel in Fig. 3. The cavity was placed on air with a ceramic gap separating it from the ultra-high vacuum (UHV) of the ring. The detection sensitivity was enhanced such that the frequency of a single ion could now be measured within a few ten milliseconds [132]. The inevitably smaller bandwidth of the detector allows for covering only 1/3 of the ESR aperture. To scan through the ring acceptance, the resonance frequency of the cavity can be varied by moving copper blocks in/out of its working volume. An identical detector is installed in the CSRe [133,134]

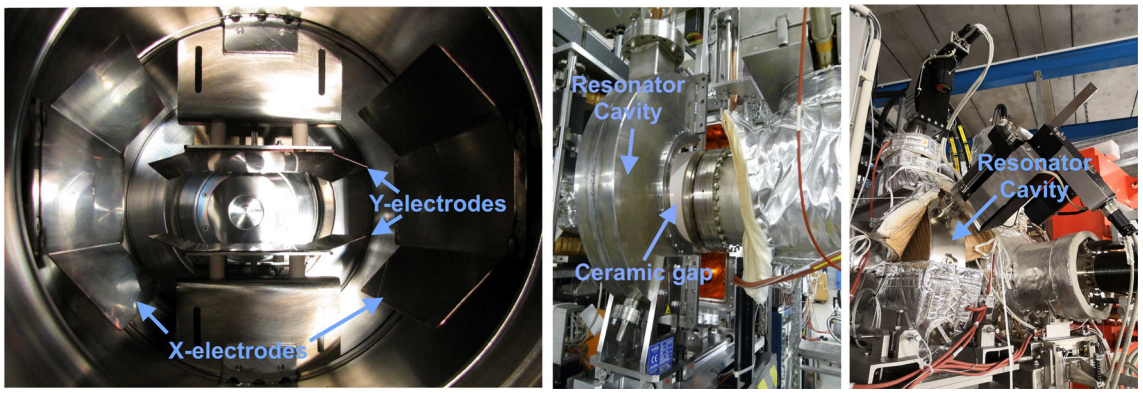


**Fig. 3** Schottky diagnostics at the ESR. Left: Two pairs of copper plates (capacitive arrangement) installed directly inside the ESR vacuum pipe [112]. Middle: First generation of resonant Schottky detector with the resonator cavity on air [113]. The cavity is screwed together around the ceramic gap. In the photo, the halves of the cavity are driven apart such that the ceramic gap (white) can be seen. Right: The recently installed fully-UHV resonant Schottky detector [114]. Photos: P. Petri, M.S. Sanjari, GSI, Darmstadt

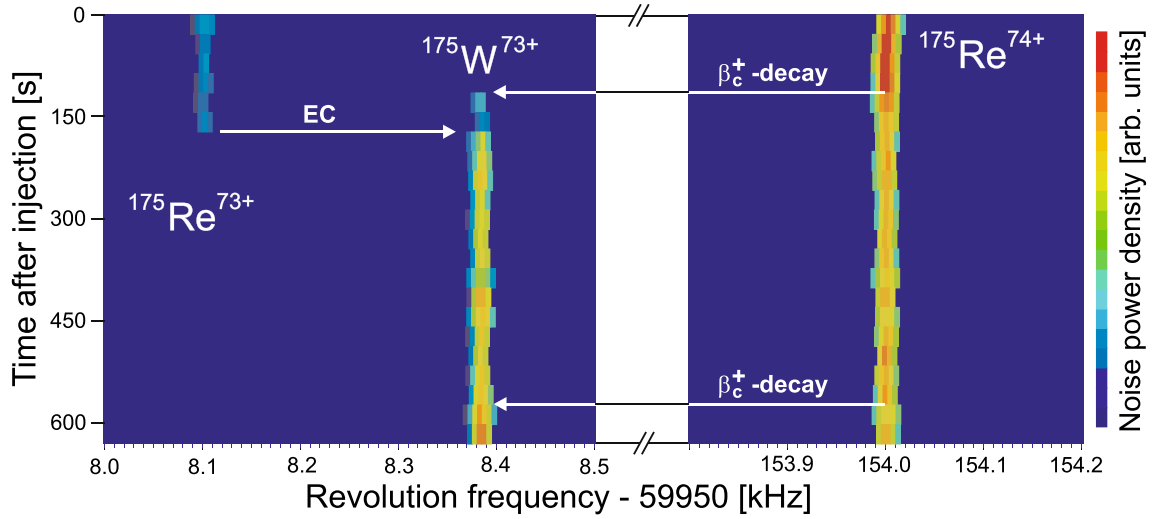


**Fig. 4** Time-resolved Schottky frequency spectra of stored isobars with $A = 175$ measured in the ESR. Data are displayed at the 30th harmonic of the mean revolution frequency of about 2 MHz, that is why the offset of 59,950 kHz is subtracted. Three H-like $^{175}W^{73+}$ ions (at $f \approx 8.4$ kHz) are produced via radioactive decays. One of them is from the EC decay of a single He-like $^{175}Re^{73+}$ ion (at $f \approx 8.1$ kHz) about 3 min after the measurement start, which is the time of the ion injection. The other two ions are products of the three-body $\beta_c^+$-decay of H-like $^{175}Re^{74+}$ ions (at $f \approx 154.0$ kHz) at about 2 and 10 min. The charge state remains the same in the EC decay and only a small $\Delta f \approx 300$ Hz is observed, which directly corresponds to the decay $Q$-value. The atomic charge state is altered by one unit in the $\beta_c^+$ decay, which yields a much larger $\Delta f \approx 140$ kHz. Note the break in the frequency scale. The figure is adopted from [41]

and, adjusted to its specific parameters, a similar one has been built for the R3 [110,111].

Figure 5 shows spectra taken with the new detector illustrating two EC decays of $^{142}Pm^{60+}$ ions [132]. Both decays have specific features associated with the kinematics of the decay. The electron cooling is always on and forces the ions to the revolution frequencies defined by their $m/q$ ratios. As discussed in Sect. 5.1, in the two-body EC decay, the energy is shared between the emitted neutrino and the recoiling daughter ion. The recoil causes a velocity mismatch, which is quickly removed by the electron cooling. This is seen by characteristic tails in Fig. 5, where the daughter nuclei require a few hundred milliseconds before they are cooled to the correct velocity, that is revolution frequency. In the first decay in Fig. 5, the electron neutrino is emitted in the backward direction. The resulting higher velocity of the daughter ion is then reduced by the cooling process, which is manifested by the right-hand side cooling tail. Vice versa, in the second decay the neutrino is emitted in the forward direction and the slower daughter ion needs to be accelerated. Since the storage ring has non-integer tune values [101], the transverse components of the recoil are averaged away after a few

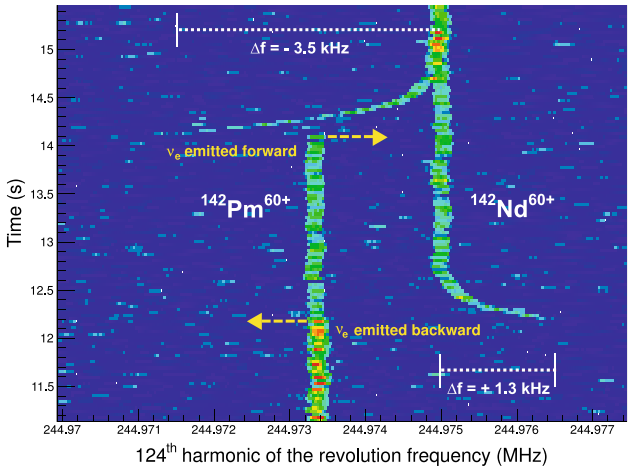


**Fig. 5** Time-resolved Schottky frequency spectra of two H-like $^{142}$Pm$^{60+}$ ions stored and electron-cooled in the ESR. Displayed is the 124th harmonic of the mean revolution frequency. Data were acquired with the resonant cavity-based Schottky detector [113], see Fig. 3 (Middle). The time- and frequency-resolutions are 32 ms and 31.25 Hz, respectively. Both parent H-like $^{142}$Pm$^{60+}$ ions decay by EC to fully-ionised $^{142}$Nd$^{60+}$ daughter nuclei, accompanied by the emission of an electron neutrino $\nu_e$. Yellow arrows indicate the true decay times, as unambiguously identified by a decrease of the intensity of the trace corresponding to the parent ions and the simultaneous onset of the trace of the recoiling daughter ion. The latter starts at a revolution frequency shifted by $\delta f$ with respect to the frequency after completion of electron cooling, which reflects the projection of the recoil velocity onto the beam direction axis immediately after the decay. The figure is adopted from [132]

revolutions. This means that the lengths of the cooling tails reflect the projections of the recoiling momenta on the beam direction axis, which, combined with the fact that the emitted neutrino is 'monochromatic', gives information on the neutrino emission angle.

In the conventional *isochronous mass spectrometry* (IMS) [118,135], the ring is tuned in a special ion-optical mode. The very principle of this mode is to send a faster ion of a given ion species onto a longer orbit while a slower ion of the same ion species onto a shorter orbit, such that the velocity spread is compensated by the lengths of the closed orbits. In this mode, the Lorentz factor of the ions $\gamma = \gamma_t$, see Eq. (1). The revolution times are measured by a time-of-flight detector. A thin foil ($\approx 10\,\mu$g/cm$^2$) is inserted into the ring aperture and is punched through by stored ions at each revolution [136–140]. Secondary electrons released from the foil provide precise timing stamps, which are then used to determine the corresponding frequencies [141,142]. Ions can accomplish several thousand revolutions before they are lost from the ring either due to the energy loss or charge-exchange reactions in the foil. The method has been primarily developed for precision mass measurements [143–157]. The fragments do not require cooling. The overall measurement takes a few hundred microseconds, which is ideally suited for addressing short-lived nuclei. However, with respect to lifetime measurements, there is an upper limit of a few $\mu$s.

### 4.2 $B\rho$-defined isochronous mass spectrometry

Due to the large velocity spread of stored ions, the condition $\gamma = \gamma_t$ is fulfilled only in a small range of $m/q$ values, termed *isochronous window*. Outside of it, the mass resolving power and–in turn–the sensitivity deteriorate rapidly [50, 158]. However, if the velocity or magnetic rigidity of each particle is known, high resolving power can be extended beyond this window [159]. This has been verified at the ESR, where, in the so-called $B\rho$-tagging regime, the rigidities of all particles were limited in the dispersive plane of the FRS by mechanical slits to about $10^{-4}$ [160]. The transmission was dramatically reduced, but the mass resolving power has increased and remained constant over the entire ESR acceptance, where at the edges of the acceptance the improvement by up to a factor of 8 was achieved. Several measurements have been conducted [161,162].

A different approach has been realised at the CSRe. Here, two ToF detectors were installed about 18 m apart in a straight section [163]. Each stored particle causes two trains of timing signals in the detectors, which are then used to determine the frequency and the velocity of each ion [164,165]. By assuming that the particles with the same $B\rho$ have the same mean $C$, a universal calibration curve can be constructed. As a result, a high mass resolving power of about 400'000 has been achieved. Furthermore, it is about constant over the entire CSRe acceptance. The widths of the frequency peaks correspond to about 5 keV/q (FWHM) [166], which means that the mass of a single ion can be determined with this precision. It is worth emphasising that the overall measurement requires merely 200 $\mu$s. A striking confirmation of the power of the method has been delivered through measurements of the masses of $^{70}$Kr and $^{75}$Sr, which were produced with rates of below 2 particles per week [167–169]. This technique was termed $B\rho$-defined IMS or $B\rho$-IMS.

At the R3, the measurement of particle velocities is realised by using standard detectors within the Big-RIPS fragment separator. The results of the first mass measurements have been reported in 2022 [107].

### 4.3 Combined isochronous + Schottky mass spectrometry

As has been discussed above, non-destructive Schottky detection is ideally suited to study exotic nuclear decays of HCIs and, indeed, it has successfully been applied to investigate long-lived ($T_{1/2} \gg 1$ s) systems, see Sect. 5. It has, however, been realised, that in order to access shorter-lived species new methods would be needed.

For instance, one could attempt to accelerate the cooling process. For this purpose stochastic and electron cool-

ing were combined. In this procedure, the fast stochastic pre-cooling reduced the momentum spread to about $10^{-4}$ within about a second. The subsequent electron cooling was then much quicker than usual and the half-life of isomeric state in $^{207}Tl^{81+}$ with $T_{1/2} = 1.33(11)$ s [170] could be measured [171,172]. No further significant decrease in the measurement time was achieved, and apart from employing it in the single-particle decay spectroscopy, see Sect. 5.1.3, this approach was no longer followed.

With the development of the new-generation of Schottky detectors[113], that enabled frequency measurement of a single stored ion within a very few ten milliseconds [132,173], it has been proposed to abandon cooling and pursue lifetime measurements in the isochronous mode [174]. Such combined Schottky+isochronous mass spectrometry (S+IMS) would comprise the advantages of both techniques. Following a proof-of-principle demonstration at the ESR [175], the S+IMS has been applied in the CSRe to measure half-lives of $^{49}Cr^{24+}$ and $^{53}Fe^{26+}$ [176], see Table 1.

To further increase the sensitivity of the Schottky detector, the ceramic gap has been removed and the cavity became a part of the beam pipe, fully integrated into the ring UHV [114], see the right panel of Fig. 3. The technique has been verified in the ESR and successfully employed to measure the two-photon de-excitation of the first exited $0^+$ state in $^{72}Ge$ [177], see Sect. 5.2. Through the development of the S+IMS, simultaneous broad-band mass and lifetime measurements can now be aimed at [178].

## 5 Experimental results

Most of the lifetime results to date were obtained with the conventional time-resolved Schottky mass spectrometry, see Sect. 4.1. It is important to emphasise that such measurements provide redundant information, since typically both, the decay of the parent ions and the growth of the number of daughter ions, are simultaneously observed. In the case of a large relative change of the magnetic rigidity in the decay, the daughter ions might leave the storage ring acceptance. In such cases, the daughter ions can be measured with in-ring particle detectors [179–181].

Employing internal gas-jet targets [182,183] facilitates atomic charge-exchange reactions, which can be used in combination with particle detectors to count the number of the produced daughter or remaining parent ions. This is essential for cases when the difference between the mass-over-charge ratios of parent and daughter ions is too small to be resolved by revolution frequency, see Sect. 5.1.2.

A careful consideration of ion losses due to atomic charge-changing reactions is necessary. The rings are operated at UHV conditions ($10^{-10}$–$10^{-12}$ mbar). Dependent on the ion species, if not limited by the radioactive decay time, the storage times can reach several hours. Collisions with the residual gas atoms and molecules as well as the recombination with the cooler electrons are the main loss mechanisms [184,185]. Furthermore, resonances in the machine can lead to unwanted losses.

Up to date results on radioactive decays of HCIs measured in heavy-ion storage rings are listed in Table 1.

### 5.1 Beta decay

Measurements of weak decays in HCIs were among the main scientific motivations for the construction of the ESR [19].

The nuclear $\beta$-decay can be expressed as: $n + \nu_e \leftrightarrow p + e^-$, where $p$, $n$, $e^-$ and $\nu_e$ indicate proton, neutron, electron and electron-neutrino, respectively. By taking into account particle-antiparticle symmetry, the following weak decays can be distinguished:

$$
\begin{aligned}
n &\rightarrow p + e^- + \bar{\nu}_e && - \text{continuum } \beta^-\text{-decay } (\beta_c^-)\\
n + \nu_e &\rightarrow p + e_b^- && - \text{bound-state } \beta^-\text{-decay } (\beta_b)\\
p &\rightarrow n + e^+ + \nu_e && - \text{continuum } \beta^+\text{-decay } (\beta_c^+)\\
p + e_b^- &\rightarrow n + \nu_e && - \text{orbital electron capture (EC)}\\
p + e^- &\rightarrow n + \nu_e && - \text{free electron capture (free EC)}
\end{aligned}
$$

Capture of free electrons is common in stellar plasmas, as e.g. $^7$Be nuclei in the Sun dominantly decay by the free electron capture from solar plasma [12,13].

#### 5.1.1 Continuum beta decay

In the continuum $\beta_c^+/\beta_c^-$ decays, the energy and momentum are shared between the three particles in the final state, namely the emitted positron/electron, neutrino/antineutrino and the recoiling daughter nucleus. Fully-ionised $^{19}Ne^{10+}$ ions were used in the first experiments at the FRS-ESR facility, during which the $\beta_c^+$ rate could be measured [39]. Short after, dedicated measurements of $\beta_c^+$ rates of fully-ionised $^{52,53}Fe^{26+}$ nuclei were conducted [186]. In these first experiments, the feasibility of decay measurements in the ESR was confirmed, thereby enabling a first comparison of the calculated and measured $\beta^+$ decay rates for fully-ionised nuclei. Continuum $\beta_c^+$ and $\beta_c^-$ decays were intensively studied in the ESR by employing the time-resolved SMS. The first application of the combined S+IMS technique was done at the CSRe, where $\beta_c^+$ rates of $^{49}Cr^{24+}$ and $^{53}Fe^{26+}$ were determined [176].

#### 5.1.2 Bound state beta decay

Bound-state beta decay [187,188] is a nuclear weak decay in which one of the neutrons $n$ in the nucleus is transmuted into a proton $p$ accompanied by the emission of an electron and an electron antineutrino. However, different from an ordinary

**Table 1** Half-lives of HCIs in ground and isomeric ($m$) states measured in storage rings. Listed are the investigated ion species, the measured or proposed decay mode, the measured half-life in the rest frame of ions ($T_{1/2}$(exp)), half-lives for neutral atoms $T_{1/2}$(lit.) are taken from NNDC [170], and NUBASE [172] evaluations the employed measurement technique, storage ring facility, and the reference to the original work, respectively. An asterisk in last column indicates a new information as compared to the table published in [38]

| Ion | Mode | $T_{1/2}$(exp) | $T_{1/2}$(lit.) | Method | | Reference | comm. |
|---|---|---|---|---|---|---|---|
| $^{19}Ne^{10+}$ | $\beta_c^+$ | 18.5(6) s[a] | 17.26(1) s | SMS | ESR | [39] | |
| $^{49}Cr^{24+}$ | $\beta_c^+$ | 44.0(27) min | 42.3(1) min | S+IMS | CSRe | [176] | * |
| $^{52m}Mn^{25+}$ | $\beta_c^+$ + IT | 22.7(30) min | 21.1(2) min | SMS | ESR | [186] | |
| $^{52}Fe^{26+}$ | $\beta_c^+$ | 12.5($^{+15}_{-12}$) h | 8.275(8) h | SMS | ESR | [186] | |
| $^{53}Fe^{26+}$ | $\beta_c^+$ | 8.5(3) min | 8.51(2) min | SMS | ESR | [186] | |
| $^{53}Fe^{26+}$ | $\beta_c^+$ | 8.47(19) min | 8.51(2) min | S+IMS | CSRe | [176] | * |
| $^{53m}Fe^{26+}$ | IT | 2.48(5) min | 2.54(2) min | SMS | ESR | [186] | |
| $^{72m}Ge^{32+}$ | $2\gamma$ | *b* | prompt | S+IMS | ESR | | * |
| $^{94m}Ru^{44+}$ | IT | 102(17) $\mu$s | 67.5(28) $\mu$s | IMS | CSRe | [229] | * |
| $^{122}I^{53+}$ | $\beta_c^+$ | 4.39(28) min | 3.63(6) min | SMS | ESR | [204] | * |
| $^{122}I^{52+}$ | $\beta_c^+$+EC | 3.27(14) min | 3.63(6) min | SMS | ESR | [204] | * |
| $^{133m}Sb^{51+}$ | IT? | $> 60\,\mu$s | 16.54(19) $\mu$s | IMS | ESR | [227,228] | |
| $^{125m}Ce^{58+}$ | IT | $130^{+64}_{-6}$s | 3.4 s (est.)[c] | SMS | ESR | [280] | |
| $^{140}Pr^{59+}$ | $\beta_c^+$ | 7.3(4) min | 3.39(1) min | SMS | ESR | [202] | |
| $^{140}Pr^{58+}$ | $\beta_c^+$+EC | 3.04(9) min | 3.39(1) min | SMS | ESR | [202] | |
| $^{140}Pr^{57+}$ | $\beta_c^+$+EC | 3.84(17) min | 3.39(1) min | SMS | ESR | [202] | |
| $^{142}Pm^{61+}$ | $\beta_c^+$ | 56.4(32) s | 40.5(5) s | SMS | ESR | [203] | |
| $^{142}Pm^{60+}$ | $\beta_c^+$+EC | 39.2(7) s | 40.5(5) s | SMS | ESR | [203] | |
| $^{142}Pm^{60+}$ | $\beta_c^+$+EC | 38.5(21) s | 40.5(5) s | SMS | ESR | [173] | * |
| $^{142}Pm^{59+}$ | $\beta_c^+$+EC | 39.6(14) s | 40.5(5) s | SMS | ESR | [203] | |
| $^{144m}Tb^{65+}$ | $\beta_c^+$ + IT | 12(2) s | 4.25(15) s | SMS | ESR | [220] | |
| $^{149m}Dy^{66+}$ | $\beta_c^+$ + IT | 11(1) s | 0.490(15) s | SMS | ESR | [220] | |
| $^{163}Dy^{66+}$ | $\beta_b^-$ | $47^{+5}_{-4}$ d | stable | SMS | ESR | [190] | |
| $^{163}Ho^{67+}$ | | stable | 4570(25) y | SMS | ESR | [190] | |
| $^{151m}Er^{68+}$ | $\beta_c^+$ + IT | 19(3) s | 0.58(2) s | SMS | ESR | [220] | |
| $^{183m}Hf^{71+}$ | $\beta_c^-$? + IT | $10^{+48}_{-5}$ s | 40(30) s | SMS | ESR | [221,222] | |
| $^{184m1}Hf^{72+}$ | IT | $1.9^{+12}_{-7}$ min | 48(10) s | SMS | ESR | [221] | |
| $^{184m1}Hf^{72+}$ | $\beta_c^-$? + IT | $113^{+60}_{-47}$ s | 48(10) s | SMS | ESR | [222] | * |
| $^{184m2}Hf^{72+}$ | $\beta_c^-$? + IT | $12^{+10}_{-4}$ min | 16(7) min | SMS | ESR | [221] | |
| $^{184m2}Hf^{72+}$ | $\beta_c^-$? | $12^{+8}_{-6}$ min | 16(7) min | SMS | ESR | [222] | * |
| $^{186m}Hf^{72+}$ | $\beta_c^-$? + IT | $> 20$ s | $> 20$ s | SMS | ESR | [221,222] | |
| $^{168}Ta^{73+}$ | $\beta_c^+$ | 5.2(7) min | 2.0(1) min | SMS | ESR | [281] | |
| $^{186m}Ta^{72+}$ | $\beta_c^-$? + IT | $3.4^{+24}_{-14}$ min | 1.54(5) min | SMS | ESR | [221] | |
| $^{186m}Ta^{72+}$ | $\beta_c^-$ + IT | $3.0^{+15}_{-8}$ min | 1.54(5) min | SMS | ESR | [222] | * |
| $^{187}Ta^{73+}$ | $\beta_c^-$ | 2.3(6) min | 2.3(6) min | SMS | ESR | [221,222] | |
| $^{187m1}Ta^{73+}$ | $\beta_c^-$? + IT | 22(9) s | 7.3(9) s | SMS | ESR | [221,222] | |
| $^{187m2}Ta^{73+}$ | $\beta_c^-$ + IT? | $> 5$ min | $> 5$ min | SMS | ESR | [221] | |
| $^{186m}W^{72+}$ | IC | $7.5^{+48}_{-33}$ s | 18(1) $\mu$s | SMS | ESR | [222] | |
| $^{187}Re^{75+}$ | $\beta_b^-$ | 32.9(20) y | 41.60(2) Gy | SMS | ESR | [191] | |
| $^{192m}Re^{75+}$ | $\beta_c^-$? + IT | $61^{+40}_{-20}$ s | $< 500$ ms | SMS | ESR | [222,223] | |

**Table 1** continued

| Ion | Mode | $T_{1/2}$(exp) | $T_{1/2}$(lit.) | Method | | Reference | comm. |
|---|---|---|---|---|---|---|---|
| $^{192m}Os^{75+}$ | $\beta_c^-$? + IT | $15.1^{+15}_{-13}$ s | 5.94(9) s | SMS | ESR | [282] | * |
| $^{195m}Os^{76+}$ | $\beta_c^-$? + IT | > 9 min | 47(3) s | SMS | ESR | [222] | |
| $^{205}Hg^{80+}$ | $\beta_c^- + \beta_b^-$ | 5.61(9) min | 5.14(9) min | SMS | ESR | [194] | |
| $^{205}Tl^{81+}$ | $\beta_b^-$ | *c* | stable | SMS | ESR | | * |
| $^{205}Pb^{82+}$ | | stable | 17.0(9) My | SMS | ESR | | * |
| $^{207}Tl^{81+}$ | $\beta_c^- + \beta_b^-$ | 4.25(19) min | 4.77(2) min | SMS | ESR | [193] | |
| $^{207}Tl^{81+}$ | $\beta_c^- + \beta_b^-$ | 4.72(19) min | 4.77(2) min | SMS | ESR | [194] | |
| $^{207m}Tl^{81+}$ | IT | 1.47(32) s | 1.33(11) s | SMS | ESR | [93,171] | |
| $^{213}Tl^{81+}$ | $\beta^-$ | $1.7^{+81}_{-8}$ min | 23.8(44) s | SMS | ESR | [283] | |
| $^{212m2}Bi^{83+}$ | IT | > 30 min | 7.0(3) min | SMS | ESR | [284] | * |
| $^{221}Po^{84+}$[d] | $\beta^-$ | $1.9^{+10}_{-5}$ min | 2.2(7) min | SMS | ESR | [283] | |
| $^{222}Po^{84+}$ | $\beta^-$ | $2.4^{+116}_{-11}$ min | 9.1(72) min | SMS | ESR | [283] | |
| $^{224}At^{85+}$[e] | $\beta^-$ | $1.3^{+23}_{-4}$ min | 2.5(15) min | SMS | ESR | [283] | |
| $^{234}Ac^{87+}$ | $\beta^-$ | 45(2) s | 45(2) s | SMS | ESR | [285] | |
| $^{235}Ac^{88+}$ | $\beta^-$ | 62(4) s | 62(4) s | SMS | ESR | [285] | |
| $^{236}Ac^{89+}$ | $\beta^-$ | $1.2^{+56}_{-6}$ min | 4.5(36) min | SMS | ESR | [283] | |

[a] 11% contamination by $\beta$-decay of $^{15}O$ is suggested in [39]
[b] Successfully measured in 2021, result is not yet disclosed
[c] Updated, see [170]
[a] Successfully measured in 2020, result is not yet disclosed
[d] Can be mixed with isobars $A = 221$ and $q = 84+$
[e] Can be mixed with isobars $A = 224$ and $q = 85+$

continuum $\beta^-$ decay mode, the electron is not emitted to the continuum but occupies one of the bound orbitals. Thus, there are two particles in the final state which share the decay $Q$-value. Two-body $\beta$-decays, EC and $\beta_b$-decay, are the time-reverse of each other. Similarly to the EC-decay in which the electron from any shell can be captured, the created electron in the bound-state $\beta^-$-decay can occupy different shells in the daughter atom. The scaling of the probabilities to capture (generate) s-electron from (in) electron shells with different principal quantum number $n$ is roughly $1/n^3$ [189]. Since the inner orbitals in neutral atoms are Pauli-blocked, $\beta_b$-decay is restricted to very weakly bound electron states of the daughter atom and is, therefore, only a marginal decay branch of neutral atoms.

Although the existence of the $\beta_b$-decay was predicted in the 1940 s [187], it took several decades until it has experimentally been verified. All results on the $\beta_b$-decay come from the ESR.

Neutral $^{163}$Dy atoms are stable and decay with half-life of about 50 days if fully ionised. This was one of the very first measurements conducted in the ESR [190]. The obtained result impacted our understanding of the *s*-process flow, where $^{163}$Dy becomes a branching point nucleus, contributing to the creation of $^{164}$Er. In turn, the observed abundance of $^{164}$Er can be used to infer the ionisation degree of $^{163}$Dy and the corresponding environment temperature [41].

In a subsequent study, the $\beta_b$-decay of fully-ionised $^{187}$Re has been measured [191]. Neutral $^{187}$Re atoms have a very long half-life of 42 Gy [170,172]. However, the increased decay $Q$-value, if all bound electrons are removed in $^{187}Re^{75+}$ ions, enables the decay to the first exited state in $^{187}$Os nucleus at $E^* = 9.8$ keV thereby reducing the half-life to merely 33 years. This result made a dramatic consequence for a possible application of the $^{187}$Re/$^{187}$Os pair as a nuclear cosmo-chronometer, turning it instead into a cosmo-thermometer [192].

The $Q$-values of the $\beta_b$-decays of $^{163}$Dy and $^{187}$Re are so small that the daughter ions cannot be resolved from the corresponding parent ions. To detect the bred H-like daughter ions an internal gas target has been utilised to strip the bound electron. The resulting bare nuclei have significantly different orbits and can be intercepted by particle detectors installed after a bending magnet downstream the target [101].

The first direct observation of the bound-state $\beta$-decay was performed on the examples of fully-ionised $^{206,207}Tl^{81+}$ nuclei, see Fig. 6. These systems have a sufficiently large decay $Q$-value (> 1 MeV), which allows for direct resolving of the parent and daughter ions by their revolution frequencies via SMS [193]. Furthermore, such large $Q$-values imply that the $\beta_c^-$-decay is also allowed. This enabled the first measurements of the $\beta_b^-/\beta_c^-$ ratios [193,194] in analogy to well

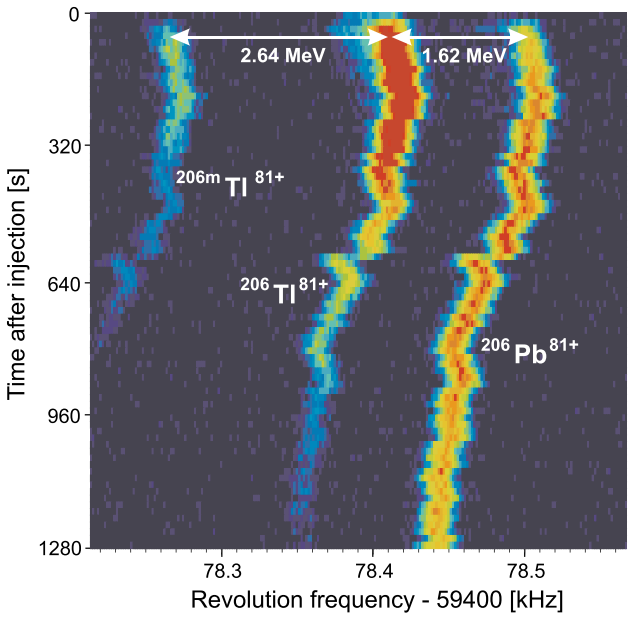


**Fig. 6** Illustration of the the bound-state beta-decay of fully-ionised $^{206}Tl^{81+}$ measured in the ESR [193,194]. The colour code represents logarithm of Schottky power in arbitrary units. Similar to Fig. 4, the data were measured at 30th harmonic of the revolution frequency. The isomeric state of thallium, labelled with *m*, decays by internal transitions to the ground state. The ground state decays via $\beta_b$ decay to H-like $^{206}Pb^{81+}$ ions. The decay *Q*-value is large enough to enable all ion species to be directly resolved. The parallel changes in the revolution frequencies are due to random fluctuations of the magnetic fields of the ESR. Figure taken from [41]

studied EC/$\beta_c^+$ branching ratios [189]. Therefrom obtained ratios are in fair agreement with theoretical estimations [30].

In spite of the successful investigations of $\beta_b$-decays, the most impactful case proposed before the construction of the ESR [195], namely the decay of $^{205}Tl^{81+}$ nuclei, remained unmeasured. The knowledge of the decay rate is essential for the conclusion on the *s*-process clockworks in the Hg-Bi region, where especially the destruction/survival of long-lived $^{205}Pb$ is affected [196]. Furthermore, there have been proposals to utilise $^{205}Tl$ as a detector for solar pp-neutrinos [197–199], where the transition strength defines the neutrino capture probability. Although $^{205}Tl$ is stable and abundant on Earth, it is poisonous and for safety reasons its use in a source was excluded. The case was revived every time an upgrade of the GSI facility was undertaken. However, the production of a sufficient amount of secondary $^{205}Tl^{81+}$ nuclei was not possible for decades. An expected half-life can lie in the range from about 50 days to about 400 days [31,32,200,201]. Therefore, $10^6 - 10^7$ ions need to be produced and stored for several hours. In 2020 the experiment has finally been accomplished. Enriched $^{206}Pb$ beam was used to produce $^{205}Tl^{81+}$ ions. A challenging complication arises from a much higher production of the $^{205}Pb^{81+}$ ions, which are the daughters of the $\beta_b$-decay of interest. Efficient production, purification, accumulation as well as the storage of up to 10 h could be achieved. The analysis is in its final stage and will be published soon.

### *5.1.3 Orbital electron capture*

On the neutron-deficient side of the nuclidic chart, the two-body beta decay mode is the orbital electron capture [189]. It is obvious that EC is disabled in fully-ionised nuclei. The number of measured EC decays in highly-charged ions is limited and all results stem from the ESR, see Table 1.

The EC decays of H- and He-like ions were measured in $^{122}_{53}I$, $^{140}_{59}Pr$, and $^{142}_{61}Pm$ ions [202–204]. Also the corresponding $\beta_c^+$ in the fully-ionised nuclei were obtained. A striking result was observed that H-like $^{140}Pr^{58+}$ and $^{142}Pm^{60+}$ ions decay through an allowed $1^+ \rightarrow 0^+$ Gamow-Teller transition by a factor ~1.5 faster than the corresponding He-like $^{140}Pr^{57+}$ and $^{142}Pm^{59+}$ ions, and even than neutral atoms. Although at first glance counterintuitive, this result could be explained by the conservation of the total angular momentum and by the fact that the ions in the ESR are stored in the ground hyperfine state [205–208]. Similar results were seen in muon capture [209] and were discussed for EC [34]. One of the consequences is that the neutrino emission direction is strictly opposite of the direction of the spin of the parent nucleus, see the discussion in relation to Fig. 5.

To verify the theoretical explanation, the Gamow-Teller $1^+ \rightarrow 2^+$ decay of H-like $^{122}_{53}I^{52+}$ ions has been studied [204]. According to the proposed selection rules, this decay shall be disabled. Indeed a slower decay has been measured. A definite conclusion though was not possible, since the decay strength is split over numerous states in the daughter nucleus [170].

Substantial research has been devoted to the verification of a surprising observation of modulated EC decay of in H-like $^{122}I^{52+}$, $^{140}Pr^{58+}$ and $^{142}Pm^{60+}$ ions [210,211]. These measurements were conducted with the so-called "single-ion decay spectroscopy", which aimed at a continuous observation of each stored ion. Precise decay times were seen as well-defined jumps of intensities corresponding to individual ions from the parent frequency to daughter frequency. Several thousands of such EC decay times were collected in several experiments. Although the periodic modulations with several second periods were not reproduced, these experiments were the motivation for the development of the highest-sensitivity Schottky detectors, see Sect. 4.1. In the latest experiment, a pure exponential decay of $^{142}Pm^{60+}$ ions was obtained with a high statistical confidence [173]. A detailed discussion of this research can be found in [212].

### 5.2 Nuclear isomers

Isomers are long-lived nuclear states [213–215]. Such states have quantum numbers, which hinder transition to the corresponding low-lying states. Isomers can de-excite either through electromagnetic channels, that is via internal conversion (IC), emission of a $\gamma$-quantum (IT), or, if the excitation energy exceeds 1.022 MeV, via the creation of an electron-positron pair, through weak channels, that is via $\beta$-decay, see Eq. (2), or through strong interaction, that is by emission of nucleons, $\alpha$-particles or fission. Conventionally, isomeric states are studied by utilising various spectroscopic methods. Of particular interest here is that highly charged ions offer a way to isolate specific decay channels.

We note, that prompt decays of excited states in HCIs can be measured at in-flight spectrometers. In such experiments, a new decay channel, namely the Bound Internal Conversion (BIC) was discovered [216–218]. Similar to the $\beta_b^-$-decay, in this IC-decay mode the conversion electron is not emitted to the continuum but transferred to a different atomic level [219].

In fully ionised nuclei, all bound electrons are removed and the de-excitation through IC is impossible. In this way the partial $(\beta^+ + \gamma)$-decay rate can be measured, which offers an independent approach to obtain conversion coefficients. In the first experiments, long-lived isomers in $^{52}$Mn and $^{53}$Fe were investigated [186] Afterwards, conversion coefficients were obtained for $^{144m}$Tb, $^{149m}$Dy and $^{151m}$Er isomeric states through measuring the pure IT channel in the corresponding fully-ionised nuclei [220]. Such measurements allow for addressing weak gamma decay branches.

A spectacular application of time-resolved SMS is to search for long-lived rarely produced isomers. Indeed, new isomeric states are frequently found in campaigns on broadband mass measurements. However, assumed here are isomeric half-lives in the order of minutes, hours or longer and production rates of one particle per hour, day, week or even smaller. Here, the ultimate sensitivity to single stored ions allows for the detection and identification of every produced rare ion. Searches for such exotic isomeric states with conventional $\gamma$-spectroscopy are very complicated. In a dedicated experiment, several high-K isomers in neutron-rich nuclides in the Hf-Os region were discovered [221–223] and their properties, like excitation energy and lifetime, were determined. The latter can then be used to specifically design a spectroscopic experiment to investigate such isomers. As an example, the isomeric state in $^{187}$Ta has been first discovered in the ESR and then thoroughly studied at the KISS facility in RIKEN [224–226].

In the last few years, the advancement in the speed and sensitivity of the newest Schottky detectors together with the development of the combined S+IMS technique provided access to nuclear lifetimes in the millisecond range. For benchmarking the power of the technique, $^{72}$Ge has been selected. The ground and first excited states in this nucleus are both $0^+$ [170]. In a fully-ionised nucleus, the IC and IT decay channels are disabled and the isomer is forced to decay via a second-order $2\gamma$-decay. The successful measurement has been conducted in 2021 and is being analysed now [177]. The results are not yet disclosed by the collaboration but are expected soon to be reported.

Last but not least, although the measurement duration in the IMS is very short, decays of $\mu$s isomers are sometimes possible to detect. Here, the large losses due to interactions of the ions with the ToF-detector foil need to be taken into account [227]. For instance, the decays of isomers in $^{133}$Sb [228] and $^{94}$Ru [229] were measured in the ESR and CSRe, respectively. The former nucleus is just one proton above the doubly-magic $^{132}$Sn and the ESR result was useful for constraining shell-model predictions in this region. In the case of $^{94}$Ru, the change of the revolution frequency due to the decay could be observed directly in the measured revolution time stamps, see Sect. 4.1.

So far obtained half-lives for isomeric states are listed in Table 1, where the assumed decay channels are indicated.

## 6 Future experiments

The rich harvest of measured half-lives presented in Table 1 shows the past successes. However, the perspectives for future measurements are as well exciting. It is important to emphasise that half-life measurements are planned at all three facilities in operation.

New experimental capabilities are coupled to advances in detector development. The major goal in the context of lifetime measurements is the ability to non-destructively determine the velocity of each stored particle in the isochronous mode. Such determination will enable all advantages of the $B\rho$-defined IMS, see Sect. 4.2. The corresponding approach is to construct transverse Schottky detectors to measure the position of each particle in a dispersive location of the ring [230–232]. This will provide the particle magnetic rigidity, from which the velocity can straightforwardly be deduced. The first prototype of such detector is being installed in the R3.

An important goal of the future measurements is a broadband determination of yet unknown $\beta$-decay half-lives. Of interest here are neutron-rich nuclei, especially those relevant to the $r$-process. There are indications that forbidden $\beta$-decays may become dominant, thus altering theoretical predictions [233,234]. An additional channel, $\beta$-delayed single-neutron ($P_{1n}$) or multiple-neutron ($P_{xn}$) emission, becomes energetically allowed in such systems [235]. Proposals to employ the combined S+IMS with telescope

detectors to measure $P_n$ values have been prepared for the ESR [236,237].

On the neutron-deficient side of the nuclidic chart, the production of nuclides beyond the proton drip-line is feasible. Taken the speed of the S+IMS, investigations of direct proton and/or $\beta$-delayed proton emission may become possible [238].

Although proposed more than 10 years ago, measurements of possible modifications of $\alpha$-decay rates in HCIs are still pending. Small changes of the rates are expected because of the reduction of the Coulomb barrier due to the missing screening effect of the electrons [239–242].

Regarding EC decays, the presently available measurement of the decay of H-like $^{122}$I [204] is yet insufficient to firmly confirm the theoretical explanation of the decay rates in H-like and He-like $^{140}$Pr and $^{142}$Pm. An ideal test candidate would be $^{111}$Sn [243], decaying by allowed Gamow-Teller transition $7/2^+ \rightarrow 9/2^+$ to the ground state of $^{111}$In, see Fig. 7. If the assumption of the disabled repopulation of hyperfine states in the storage ring is correct [244], the ground hyperfine state in H-like $^{111}$Sn has the total angular momentum $F = 3$. However, such $F$ state is not available in the daughter ion and thus the allowed $\Delta I = +1$ EC decay is not possible. We note that the magnetic moments of both nuclei are positive [170]. In the case of $^{64}$Cu it is negative [170] and thus the ordering of hyperfine states is inverted, which leads to the disabled $\Delta I = -1$ decays [245]. If experimentally

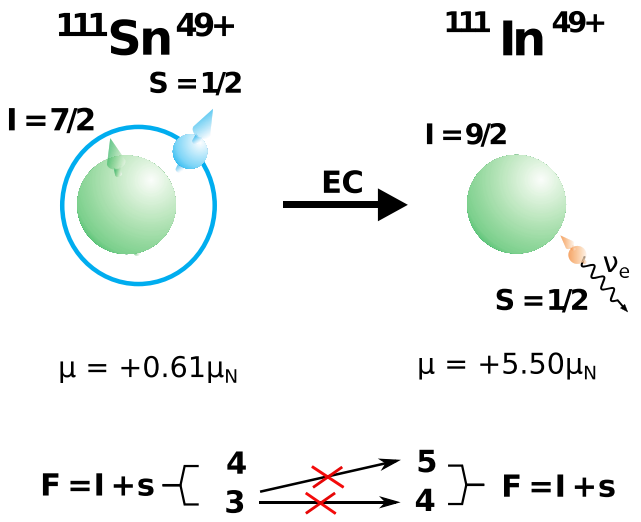


**Fig. 7** Cartoon representation of the EC decay of H-like $^{111}Sn^{49+}$ ions decaying through allowed Gamow-Teller transition to the ground state of fully-ionised $^{111}In^{49+}$ nuclei. In the initial state ($i$), the nuclear and single electron spins can couple to the total angular momenta $F_i = 3$ and $F_i = 4$. Both nuclei have positive magnetic moments [170]. After a short time, only the $F_i = 3$ hyperfine ground state is populated. No repopulation of upper hyperfine states has been observed in the ESR [244]. In the final state ($f$), the states are $F_f = 4$ and $F_f = 5$. Therefore, no $F_i = F_f$ transition is available and hence the EC decay is hindered. Taken from [247]. Courtesy Ragandeep Singh Sidhu

confirmed, it will be possible to use different combinations of states in parent and daughter nuclei to address, e.g. weak decay branches or forbidden decays, etc.

A special case is $^7$Be, which was briefly discussed in Sect. 1. The EC decay of the $3/2^-$ ground state to the $1/2^-$ first excited state in $^7$Li depends on the population of hyperfine states in $^7$Be [246]. The tiny hyperfine splitting might be used to probe the re-population probability in the storage ring.

EC decays of Li-like systems shall show similar dependence on the total angular momenta as the H-like ions. Predictions of such decays have been made and await experimental confirmation [248].

Search for long-lived rare isomers will continue. The immediate goal here is to study $^{188}$Hf where an exotic K-isomer with an exceptionally long lifetime with respect to photon decay is predicted to exist [215].

The fast S+IMS enabled half-life measurements in the millisecond range. Further measurements of known as well as yet unknown $0^+ \rightarrow 0^+$ decays are proposed at the ESR [249]. Furthermore, an exotic bound electron-positron pair decay will be addressed [250]. This decay mode is energetically open in $^{194}$Pb where the excitation energy of the first excited $0^+$ state [170] combined with the binding energy of the K-orbital [251] gives about 10 keV excess energy, which is carried away by monochromatic positrons.

Further exotic decay modes are the time-reverse of IC, termed Nuclear Excitation by (free) Electron Capture (NE(free)EC), and of BIC, termed Nuclear Excitation by Electron Transition (NEET). A large deviation was observed between the NEEC measured through depletion of the isomer in $^{93}$Mo [252] and theoretical predictions [253]. It turns out that it is crucial whether electrons are considered to be free or bound in a target atoms [254,255]. Several prepared proposals suggest various approaches to measure both NE(target)EC and NE(free)EC at the ESR and/or CRYRING@ESR [68,256,257].

Last but not least, the isomeric state in $^{229}$Th is in the focus of numerous experimental and theoretical investigations [258–260]. It is predicted that transition rates in highly charged $^{229}$Th ions may change dramatically due to the nuclear hyperfine interaction [261]. The versatile instrumentation, facilities (ESR, CRYRING@ESR, HITRAP), and variety of targets and probes offer promising prospects for studies on $^{229}$Th and other low-lying isomers [262–264].

## 7 Outlook

The presently running storage ring machines will continue research programs on half-life measurements of radioactive HCIs. However, there are several new storage ring projects launched worldwide.

At the future Facility for Antiproton and Ion Research (FAIR), which is in construction at the GSI site in Darmstadt [265], two new storage rings are planned. The first one, Collector Ring (CR), is a dedicated facility to be operated in isochronous mode [266]. It will profit from excellent design transmission from the new high-acceptance fragment separator Super-FRS [267]. Particle detectors for $P_n$ determination, a double-ToF setup, and multiple Schottky detectors will be installed thus enabling $B\rho$-defined IMS, S+IMS as well as the combination of both. Since only one ion is needed to obtain its mass and lifetime, this will be the facility, where the basic properties of the most exotic nuclei will be measured. The second ring is the High-Energy Storage Ring (HESR) [268]. Accumulation and long storage times of stochastically cooled ion beams will be possible in the HESR [269]. Counting on high intensities of secondary beams from Super-FRS and CR, dedicated measurements of rare decay channels and long half-lives are aimed at [178].

Another future complex in construction is the High Intensity Heavy-ion Accelerator Facility in China [270]. A 15 Tm spectrometer ring SRing [271] will be built behind a synchrotron, connected by the fragment separator HFRS. The multi-purpose SRing will be equipped with electron, stochastic and laser cooling capabilities, various detector and spectrometer setups, and internal targets. A special care is devoted to high quality isochronous ion-optical mode [272]. Further in the future, it is planned to upgrade the facility by adding a 45 Tm superconducting MRing [273,274], which will form a special configuration with the SRing for interaction of two co-propagating beams.

In addition to the projects in construction, there are a few ones in the discussion phase. The first one is the dedicated low-energy storage ting at ISOLDE at CERN [246]. Measurements of $\beta$-decays of HCIs is one of the proposed physics cases there. One of the key nuclei is the H-like $^7$Be, which decay probability was still not feasible to measure elsewhere. Other low-energy storage rings in discussion are the ones at LANL [275] and TRIUMF [276]. These rings will be coupled to free-neutron targets primarily for challenging neutron-induced reaction measurements [277,278], though some yet unspecified decay measurements are not excluded. Last but not least, a multi-purpose storage ring project DERICA is being considered at JINR in Dubna [279]

**Acknowledgements** We thank Filip Kondev for valuable comments. This contribution would not be possible without successful collaboration with colleagues working at the ESR, CSRe and R3. This research received support from the European Research Council (ERC) under the EU Horizon 2020 research and innovation programme (ERC-CoG "ASTRUm"), and the State of Hesse within the Research Cluster ELEMENTS (Project ID 500/10.006).

**Funding Information** Open Access funding enabled and organized by Projekt DEAL. The publication is funded by the Deutsche Forschungsgemeinschaft (DFG, German Research Foundation) - 491382106, and by the Open Access Publishing Fund of GSI Helmholtzzentrum für Schwerionenforschung.

**Data Availability Statement** This manuscript has no associated data or the data will not be deposited. [Authors' comment: This manuscript has no associated data.]



## References

1. H. Bequerel, Sur quelques observations faites avec l'uranium à de très basses températures. Compt. Rend. Acad. Sci. **133**, 199 (1901)
2. E. Rutherford, F. Soddy, LXXXIV.–The radioactivity of thorium compounds. II. The cause and nature of radioactivity. J. Chem. Soc., Trans. **81**, 837–860 (1902). https://doi.org/10.1039/CT9028100837
3. E. Rutherford, The effect of high temperature on the activity of the products of radium. Report, 77th Meeting Brit. Assoc. Advancement of Sci., 456 (1908)
4. E. Segrè, in Minutes of the Meeting at Los Angeles, California, January 3–4, 1947. Phys. Rev. **71**, 274 (1947). https://doi.org/10.1103/PhysRev.71.274
5. P.R. Daudel, Sur l'altération des périodes radioactives des éléments: A l'aide des méthodes chimiques. La Revue Scientifique **85**, 162 (1947)
6. E. Segrè, C.E. Wiegand, Experiments on the effect of atomic electrons on the decay constant of $^7$Be. Phys. Rev. **75**, 39–43 (1949). https://doi.org/10.1103/PhysRev.75.39
7. H.W. Johlige, D.C. Aumann, H.-J. Born, Determination of the relative electron density at the be nucleus in different chemical combinations, measured as changes in the electron-capture half-life of $^7$Be. Phys. Rev. C **2**, 1616–1622 (1970). https://doi.org/10.1103/PhysRevC.2.1616
8. A. Ray, P. Das, S.K. Saha et al., Observation of large change of $^7$Be decay rate in Au and $Al_2O_3$ and its implications. Phys. Lett. B **455**, 69–76 (1999). https://doi.org/10.1016/S0370-2693(99)00341-X
9. A. Ray, P. Das, S.K. Saha, S.K. Das, The effect of host medium on the half-life of $^7$Be. Phys. Lett. B **531**, 187–189 (2002). https://doi.org/10.1016/S0370-2693(02)01501-0
10. T. Ohtsuki, H. Yuki, M. Muto, J. Kasagi, K. Ohno, Enhanced electron-capture decay rate of $^7$Be encapsulated in $C_{60}$ cages. Phys. Rev. Lett. **93**, 112501 (2004). https://doi.org/10.1103/PhysRevLett.93.112501
11. A. Ray, P. Das, S.K. Saha, A. Goswami, A. De, Observation of enhanced orbital electron-capture nuclear decay rate in a compact medium. Phys. Lett. B **679**, 106–110 (2009). https://doi.org/10.1016/j.physletb.2009.07.036
12. C.W. Johnson, E. Kolbe, S.E. Koonin, K. Langanke, The fate of $^7$Be in the sun. Astroph. J. **392**, 320 (1992). https://doi.org/10.1086/171431

13. A.V. Gruzinov, J.N. Bahcall, The $^{7}$Be electron capture rate in the sun. Astroph. J. **490**, 437 (1997). https://doi.org/10.1086/304854
14. J.N. Bahcall, Electron capture and nuclear matrix elements of $^{7}$Be. Phys. Rev. **128**, 1297–1301 (1962). https://doi.org/10.1103/PhysRev.128.1297
15. J.N. Bahcall, C.P. Moeller, The $^{7}$Be electron-capture rate. Astroph. J. **155**, 511 (1969). https://doi.org/10.1086/149887
16. M.N. de Mevergnies, P. Del Marmol, Effect of the oxidation state on the half-life of $^{235m}$U. Phys. Lett. B **49**, 428–430 (1974). https://doi.org/10.1016/0370-2693(74)90626-1
17. G.T. Emery, Perturbation of nuclear decay rates. Ann. Rev. Nucl. Sci. **22**, 165–202 (1972). https://doi.org/10.1146/annurev.ns.22.120172.001121
18. S.-H. Zhou, Environmental effects on nuclear decay rates. Chin. Phys. C **35**, 449 (2011). https://doi.org/10.1088/1674-1137/35/5/008
19. P. Kienle, *Forschung Im Focus: Experimentalphysik Zwischen Abenteuer und Anwendung*. Edition Interfrom, (Zürich, Osnabrück 1993). https://www.xarg.org/ref/a/3720152499/
20. S.R. Elliott, B. Beck, P. Beiersdorfer et al., EBIT trapping program. Hyperf. Int. **81**, 151–159 (1993). https://doi.org/10.1007/BF00567259
21. K.G. Leach, I. Dillmann, R. Klawitter et al., Electroweak decay studies of highly charged radioactive ions with TITAN at TRIUMF. Atoms **5**, 14 (2017). https://doi.org/10.3390/atoms5010014
22. K.G. Leach, A. Grossheim, A. Lennarz et al., The TITAN in-trap decay spectroscopy facility at TRIUMF. Nucl. Instr. Meth. A **780**, 91–99 (2015). https://doi.org/10.1016/j.nima.2014.12.118
23. A. Lennarz, A. Grossheim, K.G. Leach et al., In-trap spectroscopy of charge-bred radioactive ions. Phys. Rev. Lett. **113**, 082502 (2014). https://doi.org/10.1103/PhysRevLett.113.082502
24. E.M. Burbidge, G.R. Burbidge, W.A. Fowler, F. Hoyle, Synthesis of the elements in stars. Rev. Mod. Phys. **29**, 547–650 (1957). https://doi.org/10.1103/RevModPhys.29.547
25. A.G.W. Cameron, Nuclear reactions in stars and nucleogenesis. Publ. Astron. Soc. Pacific **69**, 201 (1957). https://doi.org/10.1086/127051
26. H. Schatz, Nuclear masses in astrophysics. Int. J. Mass Spectrom. **349–350**, 181–186 (2013). https://doi.org/10.1016/j.ijms.2013.03.016
27. K. Langanke, H. Schatz, The role of radioactive ion beams in nuclear astrophysics. Phys. Scripta **T152**, 014011 (2013). https://doi.org/10.1088/0031-8949/2013/t152/014011
28. J.J. Cowan, C. Sneden, J.E. Lawler et al., Origin of the heaviest elements: The rapid neutron-capture process. Rev. Mod. Phys. **93**, 015002 (2021). https://doi.org/10.1103/RevModPhys.93.015002
29. J.N. Bahcall, Beta decay in stellar interiors. Phys. Rev. **126**, 1143–1149 (1962). https://doi.org/10.1103/PhysRev.126.1143
30. K. Takahashi, K. Yokoi, Nuclear $\beta$-decays of highly ionized heavy atoms in stellar interiors. Nucl. Phys. A **404**, 578–598 (1983). https://doi.org/10.1016/0375-9474(83)90277-4
31. K. Takahashi, R.N. Boyd, G.J. Mathews, K. Yokoi, Bound-state beta decay of highly ionized atoms. Phys. Rev. C **36**, 1522–1528 (1987). https://doi.org/10.1103/PhysRevC.36.1522
32. K. Takahashi, K. Yokoi, Beta-decay rates of highly ionized heavy atoms in stellar interiors. At. Data Nucl. Data Tab. **36**, 375–409 (1987). https://doi.org/10.1016/0092-640X(87)90010-6
33. B. Arad, S. Eliezer, Y. Paiss, Nuclear "anti-Stokes" transitions induced by laser radiation. Phys. Lett. A **74**, 395–397 (1979). https://doi.org/10.1016/0375-9601(79)90234-2
34. L.M. Folan, V.I. Tsifrinovich, Effects of the hyperfine interaction on orbital electron capture. Phys. Rev. Lett. **74**, 499–501 (1995). https://doi.org/10.1103/PhysRevLett.74.499
35. F.F. Karpeshin, Electron shell as a resonator. Hyperf. Int. **143**, 79–96 (2002). https://doi.org/10.1023/A:1024056828718
36. A. Pálffy, Nuclear effects in atomic transitions. Contemp. Phys. **51**, 471–496 (2010). https://doi.org/10.1080/00107514.2010.493325
37. P. Indelicato, QED tests with highly charged ions. J. Phys. B **52**, 232001 (2019). https://doi.org/10.1088/1361-6455/ab42c9
38. B. Singh, Y.A. Litvinov, Half-lives of fully-ionized (bare) and highly-charged atoms. In: Tuli, J.K. (ed.) Nuclear Wallet Cards, Brookhaven National Laboratory, U. S. A. (2011). https://www.nndc.bnl.gov/wallet/wall35.pdf
39. H. Geissel, K. Beckert, F. Bosch et al., First storage and cooling of secondary heavy-ion beams at relativistic energies. Phys. Rev. Lett. **68**, 3412–3415 (1992). https://doi.org/10.1103/PhysRevLett.68.3412
40. C. Scheidenberger, T. Stöhlker, W.E. Meyerhof et al., Charge states of relativistic heavy ions in matter. Nucl. Instr. Meth. B **142**, 441–462 (1998). https://doi.org/10.1016/S0168-583X(98)00244-4
41. Y.A. Litvinov, F. Bosch, Beta decay of highly charged ions. Rep. Prog. Phys. **74**, 016301 (2011). https://doi.org/10.1088/0034-4885/74/1/016301
42. U. Köster, Intense radioactive-ion beams produced with the ISOL method. Eur. Phys. J. A **15**, 255–263 (2002). https://doi.org/10.1140/epja/i2001-10264-2
43. C.A. Bertulani, P. Danielewicz, *Introduction to Nuclear Reactions* (CRC Press, Boca Raton, 2021). https://doi.org/10.1201/9780429331060
44. R.E. Marrs, S.R. Elliott, D.A. Knapp, Production and trapping of hydrogenlike and bare uranium ions in an electron beam ion trap. Phys. Rev. Lett. **72**, 4082–4085 (1994). https://doi.org/10.1103/PhysRevLett.72.4082
45. F. Wenander, Charge breeding techniques. Nucl. Phys. A **746**, 40–46 (2004). https://doi.org/10.1016/j.nuclphysa.2004.09.016
46. F. Wenander, Charge breeding of radioactive ions with EBIS and EBIT. J. Instr. **5**, 10004 (2010). https://doi.org/10.1088/1748-0221/5/10/C10004
47. J. Dilling, P. Bricault, M. Smith, H.-J. Kluge, The proposed TITAN facility at ISAC for very precise mass measurements on highly charged short-lived isotopes. Nucl. Instr. Meth. B **204**, 492–496 (2003). https://doi.org/10.1016/S0168-583X(02)02118-3
48. K. Blaum, High-accuracy mass spectrometry with stored ions. Phys. Rep. **425**, 1–78 (2006). https://doi.org/10.1016/j.physrep.2005.10.011
49. F. Herfurth, Z. Andelkovic, W. Barth et al., The HITRAP facility for slow highly charged ions. Phys. Scripta **T166**, 014065 (2015). https://doi.org/10.1088/0031-8949/2015/t166/014065
50. Y.H. Zhang, Y.A. Litvinov, T. Uesaka, H.S. Xu, Storage ring mass spectrometry for nuclear structure and astrophysics research. Phys. Scripta **91**, 073002 (2016). https://doi.org/10.1088/0031-8949/91/7/073002
51. T. Yamaguchi, H. Koura, Y.A. Litvinov, M. Wang, Masses of exotic nuclei. Prog. Part. Nucl. Phys. **120**, 103882 (2021). https://doi.org/10.1016/j.ppnp.2021.103882
52. H. Geissel, G. Münzenberg, K. Riisager, Secondary exotic nuclear beams. Ann. Rev. Nucl. Part. Sci. **45**, 163–203 (1995). https://doi.org/10.1146/annurev.ns.45.120195.001115
53. H. Geissel, H. Weick, C. Scheidenberger, R. Bimbot, D. Gardès, Experimental studies of heavy-ion slowing down in matter. Nucl. Instr. Meth. B **195**, 3–54 (2002). https://doi.org/10.1016/S0168-583X(02)01311-3
54. M. Lochmann, R. Jöhren, C. Geppert et al., Observation of the hyperfine transition in lithium-like bismuth $^{209}Bi^{80+}$: Towards a test of QED in strong magnetic fields. Phys. Rev. A **90**, 030501 (2014). https://doi.org/10.1103/PhysRevA.90.030501
55. J. Ullmann, Z. Andelkovic, C. Brandau et al., High precision hyperfine measurements in Bismuth challenge bound-state

strong-field QED. Nat. Comm. **8**, 15484 (2017). https://doi.org/10.1038/ncomms15484
56. V.P. Shevelko, N. Winckler, I.Y. Tolstikhina, Stripping of relativistic uranium-ion beams by foils. Nucl. Instr. Meth. B **479**, 23–34 (2020). https://doi.org/10.1016/j.nimb.2020.06.020
57. V.P. Shevelko, N. Winckler, I.Y. Tolstikhina, Charge-state distributions of relativistic gold-ion beams stripped by foils. Phys. Rev. A **101**, 012704 (2020). https://doi.org/10.1103/PhysRevA.101.012704
58. H. Weick, A.H. Sörensen, H. Geissel et al., Energy-loss straggling of (200–1000) MeV/u uranium ions. Nucl. Instr. Meth. B **193**, 1–7 (2002). https://doi.org/10.1016/S0168-583X(02)00718-8
59. B. Franzke, H. Geissel, G. Münzenberg, Mass and lifetime measurements of exotic nuclei in storage rings. Mass Spectr. Rev. **27**, 428–469 (2008). https://doi.org/10.1002/mas.20173
60. H. Geissel, T. Schwab, P. Armbruster et al., Ions penetrating through ion-optical systems and matter—non-Liouvillian phase-space modelling. Nucl. Instr. Meth. A **282**, 247–260 (1989). https://doi.org/10.1016/0168-9002(89)90148-4
61. H. Geissel, P. Armbruster, K.H. Behr et al., The GSI projectile fragment separator (FRS): a versatile magnetic system for relativistic heavy ions. Nucl. Instr. Meth. B **70**, 286–297 (1992). https://doi.org/10.1016/0168-583X(92)95944-M
62. Y.A. Litvinov, H. Geissel, K. Beckert et al., Direct mass measurements of neutron-deficient $^{152}$Sm projectile fragments at the FRS-ESR facility. Hyperf. Int. **173**, 55–60 (2006). https://doi.org/10.1007/s10751-007-9542-3
63. D. Atanasov, K. Blaum, F. Bosch et al., Between atomic and nuclear physics: Radioactive decays of highly-charged ions. J. Phys. B **48**, 144024 (2015). https://doi.org/10.1088/0953-4075/48/14/144024
64. Y.A. Litvinov, S. Bishop, K. Blaum et al., Nuclear physics experiments with ion storage rings. Nucl. Instr. Meth. B **317**, 603–616 (2013). https://doi.org/10.1016/j.nimb.2013.07.025
65. K. Blasche, D. Bohne, B. Franzke, H. Prange, The SIS heavy ion synchrotron project. IEEE Transact. Nucl. Sci. **32**, 2657–2661 (1985). https://doi.org/10.1109/TNS.1985.4334010
66. B. Franzke, The heavy ion storage and cooler ring project ESR at GSI. Nucl. Instr. Meth. B **24–25**, 18–25 (1987). https://doi.org/10.1016/0168-583X(87)90583-0
67. M. Lestinsky, A. Bräuning-Demian, H. Danared et al., CRYRING@ESR: present status and future research. Phys. Scripta **T166**, 014075 (2015). https://doi.org/10.1088/0031-8949/2015/T166/014075
68. M. Lestinsky, V. Andrianov, B. Aurand et al., Physics book: CRYRING@ESR. Eur. Phys. J. Special Topics **225**, 797–882 (2016). https://doi.org/10.1140/epjst/e2016-02643-6
69. H.-J. Kluge, T. Beier, K. Blaum et al., HITRAP: A facility at GSI for highly charged ions. Adv. Quant. Chem. **53**, 83–98 (2008). https://doi.org/10.1016/S0065-3276(07)53007-8
70. Q. Zhong, T. Aumann, S. Bishop et al., $^{96}$Ru(p,$\gamma$)$^{97}$Rh measurement at the GSI storage ring. J. Phys. Conf. Series **202**, 012011 (2010). https://doi.org/10.1088/1742-6596/202/1/012011
71. B. Mei, T. Aumann, S. Bishop et al., First measurement of the $^{96}$Ru($p$, $\gamma$)$^{97}$Rh cross section for the $p$ process with a storage ring. Phys. Rev. C **92**, 035803 (2015). https://doi.org/10.1103/PhysRevC.92.035803
72. D.T. Doherty, P.J. Woods, Y.A. Litvinov et al., Nuclear transfer reaction measurements at the ESR for the investigation of the astrophysical $^{15}$O($\alpha$,$\gamma$)$^{19}$Ne reaction. Phys. Scripta **T166**, 014007 (2015). https://doi.org/10.1088/0031-8949/2015/t166/014007
73. J.C. Zamora, T. Aumann, S. Bagchi et al., First measurement of isoscalar giant resonances in a stored-beam experiment. Phys. Lett. B **763**, 16–19 (2016). https://doi.org/10.1016/j.physletb.2016.10.015
74. J.C. Zamora, T. Aumann, S. Bagchi et al., Nuclear-matter radius studies from $^{58}$Ni($\alpha$, $\alpha$) experiments at the GSI Experimental Storage Ring with the EXL facility. Phys. Rev. C **96**, 034617 (2017). https://doi.org/10.1103/PhysRevC.96.034617
75. J. Glorius, C. Langer, Z. Slavkovská et al., Approaching the gamow window with stored ions: direct measurement of $^{124}$Xe($p$, $\gamma$) in the ESR storage ring. Phys. Rev. Lett. **122**, 092701 (2019). https://doi.org/10.1103/PhysRevLett.122.092701
76. C. Brandau, C. Kozhuharov, A. Müller et al., Isotope shifts in dielectronic recombination: From stable to in-flight-produced nuclei. J. Phys. Conf. Ser. **194**, 012023 (2009). https://doi.org/10.1088/1742-6596/194/1/012023
77. C. Brandau, C. Kozhuharov, A. Müller et al., Resonant recombination at ion storage rings: a conceptual alternative for isotope shift and hyperfine studies. Hyperf. Int. **196**, 115–127 (2010). https://doi.org/10.1007/s10751-009-0142-2
78. C. Brandau, C. Kozhuharov, A. Müller et al., Probing nuclear properties by resonant atomic collisions between electrons and ions. Phys. Scripta **T156**, 014050 (2013). https://doi.org/10.1088/0031-8949/2013/t156/014050
79. J.W. Xia, W.L. Zhan, B.W. Wei et al., The heavy ion cooler-storage-ring project (HIRFL-CSR) at Lanzhou. Nucl. Instr. Meth. A **488**, 11–25 (2002). https://doi.org/10.1016/S0168-9002(02)00475-8
80. L.J. Mao, J.C. Yang, W.Q. Yang et al., Introduction of the heavy ion research facility in Lanzhou (HIRFL). J. Instr. **15**, 12015 (2020). https://doi.org/10.1088/1748-0221/15/12/T12015
81. Y. Litvinov, H. Geissel, R. Knöbel, B. Sun, H. Xu, Direct mass measurements of exotic nuclei in storage rings. Acta Phys. Polon. B **41**, 511–523 (2010)
82. Y.J. Yuan, L.T. Sun, J.C. Yang, et al. Status and upgrades of HIRFL. In: 13th Int. Conf. on Heavy Ion Accelerator Technology, pp. 1–01 (2016). https://doi.org/10.18429/JACoW-HIAT2015-TUM1I01
83. I. Meshkov, Storage and cooling of ion beams. Phys. Scripta **T166**, 014037 (2015). https://doi.org/10.1088/0031-8949/2015/T166/014037
84. H. Poth, Electron cooling: Theory, experiment, application. Phys. Rep. **196**, 135–297 (1990). https://doi.org/10.1016/0370-1573(90)90040-9
85. D. Möhl, G. Petrucci, L. Thorndahl, S. van der Meer, Physics and technique of stochastic cooling. Phys. Rep. **58**, 73–102 (1980). https://doi.org/10.1016/0370-1573(80)90140-4
86. M. Steck, P. Beller, K. Beckert, B. Franzke, F. Nolden, Electron cooling experiments at the ESR. Nucl. Instr. Meth. A **532**, 357–365 (2004). https://doi.org/10.1016/j.nima.2004.06.065
87. F. Nolden, K. Beckert, P. Beller, B. Franzke, C. Peschke, M. Steck, Experience and prospects of stochastic cooling of radioactive beams at GSI. Nucl. Instr. Meth. A **532**, 329–334 (2004). https://doi.org/10.1016/j.nima.2004.06.062
88. Y. Xiao-Dong, M. Li-Jun, L. Guo-Hong et al., Commissioning of electron cooling in CSRe. Chin. Phys. C **34**, 998 (2010). https://doi.org/10.1088/1674-1137/34/7/013
89. G.Y. Zhu, J.X. Wu, F. Caspers et al., Stochastic cooling experiments for CSRe at IMP. Nucl. Instr. Meth. A **932**, 83–89 (2019). https://doi.org/10.1016/j.nima.2018.09.023
90. S. Schröder, R. Klein, N. Boos et al., First laser cooling of relativistic ions in a storage ring. Phys. Rev. Lett. **64**, 2901–2904 (1990). https://doi.org/10.1103/PhysRevLett.64.2901
91. D. Winters, T. Beck, G. Birkl et al., Laser cooling of relativistic heavy-ion beams for FAIR. Phys. Scripta **T166**, 014048 (2015). https://doi.org/10.1088/0031-8949/2015/T166/014048
92. W. Wen, H. Wang, Z. Huang et al., Laser cooling and precision laser spectroscopy of highly charged ions at the storage ring CSRe and the future HIAF. Hyperf. Int. **240**, 45 (2019). https://doi.org/10.1007/s10751-019-1583-x

93. F. Bosch, H. Geissel, Y.A. Litvinov et al., Experiments with stored exotic nuclei at relativistic energies. Int. J. Mass Spectrom. **251**, 212–219 (2006). https://doi.org/10.1016/j.ijms.2006.01.037
94. F. Bosch, Y.A. Litvinov, T. Stöhlker, Nuclear physics with unstable ions at storage rings. Prog. Part. Nucl. Phys. **73**, 84–140 (2013). https://doi.org/10.1016/j.ppnp.2013.07.002
95. T. Stöhlker, Y.A. Litvinov, A. Bräuning-Demian et al., SPARC collaboration: new strategy for storage ring physics at FAIR. Hyperf. Int. **227**, 45–53 (2014). https://doi.org/10.1007/s10751-014-1047-2
96. P. Woods, K. Blaum, F. Bosch, M. Heil, Y.A. Litvinov, R. Reifarth, Nuclear astrophysics experiments at storage rings: midterm perspectives at GSI. Phys. Scripta **T166**, 014002 (2015). https://doi.org/10.1088/0031-8949/2015/t166/014002
97. T. Stöhlker, V. Bagnoud, K. Blaum et al., APPA at FAIR: From fundamental to applied research. Nucl. Instr. Meth. B **365**, 680–685 (2015). https://doi.org/10.1016/j.nimb.2015.07.077
98. W. Nörtershäuser, R. Sánchez, Laser spectroscopy at storage rings. Phys. Scripta **T166**, 014020 (2015). https://doi.org/10.1088/0031-8949/2015/T166/014020
99. J.T. Zhang, K. Yue, H.X. Li et al., The development of in-ring reaction measurements at the HIRFL-CSR. Nucl. Instr. Meth. A **948**, 162848 (2019). https://doi.org/10.1016/j.nima.2019.162848
100. P. Egelhof, The EXL Project – Present Status and Future Perspectives at FAIR. JPS Conf. Proc. **35**, 011002. https://doi.org/10.7566/JPSCP.35.011002
101. M. Steck, Y.A. Litvinov, Heavy-ion storage rings and their use in precision experiments with highly charged ions. Prog. Part. Nucl. Phys. **115**, 103811 (2020). https://doi.org/10.1016/j.ppnp.2020.103811
102. X. Ma, S. Zhang, W. Wen et al., Atomic structure and collision dynamics with highly charged ions. Chin. Phys. B **31**, 093401 (2022). https://doi.org/10.1088/1674-1056/ac8736
103. Y.A. Litvinov, J. Glorius, T. Stöhlker, et al. Precision experiments with heavy-ion storage rings. Acta Phys. Pol. B Proc. Suppl. **16**, 4–A25 (2023). https://doi.org/10.5506/APhysPolBSupp.16.4-A25
104. A. Ozawa, T. Uesaka, M. Wakasugi et al., The rare-RI ring. Prog. Theor. Exp. Phys. **2012**, 03–009 (2012). https://doi.org/10.1093/ptep/pts060
105. Y. Yamaguchi, M. Wakasugi, T. Uesaka et al., Construction of rare-RI ring at RIKEN RI Beam Factory. Nucl. Instr. Meth. B **317**, 629–635 (2013). https://doi.org/10.1016/j.nimb.2013.06.004
106. T. Yamaguchi, Y. Yamaguchi, A. Ozawa, The challenge of precision mass measurements of short-lived exotic nuclei: Development of a new storage ring mass spectrometry. Int. J. Mass Spectrom. **349–350**, 240–246 (2013). https://doi.org/10.1016/j.ijms.2013.04.027
107. H.F. Li, S. Naimi, T.M. Sprouse et al., First application of mass measurements with the Rare-RI Ring reveals the solar $r$-process abundance trend at $A = 122$ and $A = 123$. Phys. Rev. Lett. **128**, 152701 (2022). https://doi.org/10.1103/PhysRevLett.128.152701
108. T. Kubo, D. Kameda, H. Suzuki et al., BigRIPS separator and ZeroDegree spectrometer at RIKEN RI Beam Factory. Prog. Theor. Exp. Phys. **2012**, 03–003 (2012). https://doi.org/10.1093/ptep/pts064
109. Y. Yamaguchi, H. Miura, M. Wakasugi et al., Fast-kicker system for rare-RI ring. Phys. Scripta **T166**, 014056 (2015). https://doi.org/10.1088/0031-8949/2015/T166/014056
110. F. Suzaki, Y. Abe, A. Ozawa et al., A resonant Schottky pick-up for Rare-RI Ring at RIKEN. Phys. Scripta **T166**, 014059 (2015). https://doi.org/10.1088/0031-8949/2015/T166/014059
111. F. Suzaki, J. Zenihiro, T. Yamaguchi et al., Design study of a resonant Schottky pick-up for the Rare-RI Ring project. Nucl. Instr. Meth. B **317**, 636–639 (2013). https://doi.org/10.1016/j.nimb.2013.07.062
112. U. Schaaf, Schottky-Diagnose und BTF-Messungen an Gekühlten Strahlen im Schwerionenspeicherring ESR. PhD thesis, Universisity of Frankfurt (1991)
113. F. Nolden, P. Hülsmann, Y.A. Litvinov et al., A fast and sensitive resonant Schottky pick-up for heavy ion storage rings. Nucl. Instr. Meth. A **659**, 69–77 (2011). https://doi.org/10.1016/j.nima.2011.06.058
114. M.S. Sanjari, D. Dmytriiev, Y.A. Litvinov et al., A 410 MHz resonant cavity pickup for heavy ion storage rings. Rev. Sci. Instr. **91**, 083303 (2020). https://doi.org/10.1063/5.0009094
115. H. Wollnik, Principles of time-of-flight mass analyzers. Nucl. Instr. Meth. A **298**, 156–160 (1990). https://doi.org/10.1016/0168-9002(90)90611-9
116. H. Wollnik, Energy-isochronous time-of-flight mass analyzers. Int. J. Mass Spectrom. Ion Proc. **131**, 387–407 (1994). https://doi.org/10.1016/0168-1176(93)03888-S
117. T. Radon, T. Kerscher, B. Schlitt et al., Schottky mass measurements of cooled proton-rich nuclei at the GSI experimental storage ring. Phys. Rev. Lett. **78**, 4701–4704 (1997). https://doi.org/10.1103/PhysRevLett.78.4701
118. M. Hausmann, F. Attallah, K. Beckert et al., First isochronous mass spectrometry at the experimental storage ring ESR. Nucl. Instr. Meth. A **446**, 569–580 (2000). https://doi.org/10.1016/S0168-9002(99)01192-4
119. X.L. Yan, F. Bosch, Y.A. Litvinov et al., Investigation of the momentum compaction factor of the ESR through Schottky mass measurements. Phys. Scripta **T166**, 014045 (2015). https://doi.org/10.1088/0031-8949/2015/T166/014045
120. M. Zhang, Y.H. Zhang, M. Wang et al., Precision measurement of the transition energy $\gamma_t$ versus magnetic rigidity for storage-ring isochronous mass spectrometry. Nucl. Instr. Meth. A **1027**, 166329 (2022). https://doi.org/10.1016/j.nima.2022.166329
121. T. Radon, H. Geissel, G. Münzenberg et al., Schottky mass measurements of stored and cooled neutron-deficient projectile fragments in the element range of $57 \leq Z \leq 84$. Nucl. Phys. A **677**, 75–99 (2000). https://doi.org/10.1016/S0375-9474(00)00304-3
122. H. Geissel, Y.A. Litvinov, K. Beckert et al., Present and future experiments with stored exotic nuclei at the FRS-ESR facility. Eur. Phys. J. Special Topics **150**, 109–115 (2007). https://doi.org/10.1140/epjst/e2007-00280-x
123. M. Steck, K. Beckert, H. Eickhoff, B. Franzke, F. Nolden, H. Reich, B. Schlitt, T. Winkler, Anomalous temperature reduction of electron-cooled heavy ion beams in the storage ring ESR. Phys. Rev. Lett. **77**, 3803–3806 (1996). https://doi.org/10.1103/PhysRevLett.77.3803
124. Y.A. Litvinov, F. Attallah, K. Beckert et al., Schottky mass measurements of cooled exotic nuclei. Hyperf. Int. **132**, 281–287 (2001). https://doi.org/10.1023/A:1011907602706
125. Y.N. Novikov, F. Attallah, F. Bosch et al., Mass mapping of a new area of neutron-deficient suburanium nuclides. Nucl. Phys. A **697**, 92–106 (2002). https://doi.org/10.1016/S0375-9474(01)01233-7
126. Y.A. Litvinov, H. Geissel, T. Radon et al., Mass measurement of cooled neutron-deficient bismuth projectile fragments with time-resolved Schottky mass spectrometry at the FRS-ESR facility. Nucl. Phys. A **756**, 3–38 (2005). https://doi.org/10.1016/j.nuclphysa.2005.03.015
127. Y.A. Litvinov, T.J. Bürvenich, H. Geissel et al., Isospin dependence in the odd-even staggering of nuclear binding energies. Phys. Rev. Lett. **95**, 042501 (2005). https://doi.org/10.1103/PhysRevLett.95.042501
128. L. Chen, Y.A. Litvinov, W.R. Plass et al., Schottky mass measurement of the $^{208}$Hg isotope: implication for the Proton-Neutron interaction strength around doubly magic $^{208}$Pb. Phys. Rev. Lett. **102**, 122503 (2009). https://doi.org/10.1103/PhysRevLett.102.122503

129. L. Chen, W.R. Plass, H. Geissel et al., New results on mass measurements of stored neutron-rich nuclides in the element range from Pt to U with the FRS-ESR facility at 360–400 MeV/u. Nucl. Phys. A **882**, 71–89 (2012). https://doi.org/10.1016/j.nuclphysa.2012.03.002
130. D. Shubina, R.B. Cakirli, Y.A. Litvinov et al., Schottky mass measurements of heavy neutron-rich nuclides in the element range $70 \leq Z \leq 79$ at the GSI experimental storage ring. Phys. Rev. C **88**, 024310 (2013). https://doi.org/10.1103/PhysRevC.88.024310
131. Y.A. Litvinov, H. Geissel, Y.N. Novikov et al., Precision experiments with time-resolved Schottky mass spectrometry. Nucl. Phys. A **734**, 473–476 (2004). https://doi.org/10.1016/j.nuclphysa.2004.01.089
132. P. Kienle, F. Bosch, P. Bühler et al., High-resolution measurement of the time-modulated orbital electron capture and of the $\beta^+$ decay of hydrogen-like $^{142}Pm^{60+}$ ions. Phys. Lett. B **726**, 638–645 (2013). https://doi.org/10.1016/j.physletb.2013.09.033
133. Y.D. Zhang, J.X. Wu, T.C. Zhao et al., Simulation and measurement of the resonant Schottky pickup. Chin. Phys. C **35**, 1124 (2011). https://doi.org/10.1088/1674-1137/35/12/008
134. J.X. Wu, Y.D. Zang, F. Nolden et al., Performance of the resonant Schottky pickup at CSRe. Nucl. Instr. Meth. B **317**, 623–628 (2013). https://doi.org/10.1016/j.nimb.2013.08.017
135. M. Hausmann, J. Stadlmann, F. Attallah et al., Isochronous mass measurements of hot exotic nuclei. Hyperf. Int. **132**, 289–295 (2001). https://doi.org/10.1023/A:1011911720453
136. J. Trötscher, K. Balog, H. Eickhoff et al., Mass measurements of exotic nuclei at the ESR. Nucl. Instr. Meth. B **70**, 455–458 (1992). https://doi.org/10.1016/0168-583X(92)95965-T
137. B. Mei, X. Tu, M. Wang et al., A high performance time-of-flight detector applied to isochronous mass measurement at CSRe. Nucl. Instr. Meth. A **624**, 109–113 (2010). https://doi.org/10.1016/j.nima.2010.09.001
138. W. Zhang, X.L. Tu, M. Wang et al., Time-of-flight detectors with improved timing performance for isochronous mass measurements at the CSRe. Nucl. Instr. Meth. A **756**, 1–5 (2014). https://doi.org/10.1016/j.nima.2014.04.051
139. W. Zhang, X.L. Tu, M. Wang et al., A timing detector with pulsed high-voltage power supply for mass measurements at CSRe. Nucl. Instr. Meth. A **755**, 38–43 (2014). https://doi.org/10.1016/j.nima.2014.04.031
140. N. Kuzminchuk-Feuerstein, B. Fabian, M. Diwisch et al., Efficiency and rate capability studies of the time-of-flight detector for isochronous mass measurements of stored short-lived nuclei with the FRS-ESR facility. Nucl. Instr. Meth. A **821**, 160–168 (2016). https://doi.org/10.1016/j.nima.2016.03.036
141. X.L. Tu, M. Wang, Y.A. Litvinov et al., Precision isochronous mass measurements at the storage ring CSRe in Lanzhou. Nucl. Instr. Meth. A **654**, 213–218 (2011). https://doi.org/10.1016/j.nima.2011.07.018
142. Y.M. Xing, Y.H. Zhang, M. Wang et al., Particle identification and revolution time corrections for the isochronous mass spectrometry in storage rings. Nucl. Instr. Meth. A **941**, 162331 (2019). https://doi.org/10.1016/j.nima.2019.06.072
143. J. Stadlmann, M. Hausmann, F. Attallah et al., Direct mass measurement of bare short-lived $^{44}$V, $^{48}$Mn, $^{41}$Ti and $^{45}$Cr ions with isochronous mass spectrometry. Phys. Lett. B **586**, 27–33 (2004). https://doi.org/10.1016/j.physletb.2004.02.014
144. B. Sun, R. Knöbel, Y.A. Litvinov et al., Nuclear structure studies of short-lived neutron-rich nuclei with the novel large-scale isochronous mass spectrometry at the FRS-ESR facility. Nucl. Phys. A **812**, 1–12 (2008). https://doi.org/10.1016/j.nuclphysa.2008.08.013
145. X.L. Tu, H.S. Xu, M. Wang et al., Direct mass measurements of short-lived $A = 2Z - 1$ nuclides $^{63}$Ge,$^{65}$ As, $^{67}$Se, and $^{71}$Kr and their impact on nucleosynthesis in the $rp$ process. Phys. Rev. Lett. **106**, 112501 (2011). https://doi.org/10.1103/PhysRevLett.106.112501
146. Y.H. Zhang, H.S. Xu, Y.A. Litvinov et al., Mass measurements of the neutron-deficient $^{41}$Ti,$^{45}$ Cr, $^{49}$Fe, and $^{53}$Ni nuclides: First test of the isobaric multiplet mass equation in $fp$-shell nuclei. Phys. Rev. Lett. **109**, 102501 (2012). https://doi.org/10.1103/PhysRevLett.109.102501
147. X.L. Yan, H.S. Xu, Y.A. Litvinov et al., Mass measurement of $^{45}$Cr and its impact on the Ca-Sc cycle in x-ray bursts. Astroph. J. Lett. **766**, L8 (2013). https://doi.org/10.1088/2041-8205/766/1/l8
148. P. Shuai, H.S. Xu, X.L. Tu et al., Charge and frequency resolved isochronous mass spectrometry and the mass of $^{51}$Co. Phys. Lett. B **735**, 327–331 (2014). https://doi.org/10.1016/j.physletb.2014.06.046
149. X. Xu, P. Zhang, P. Shuai et al., Identification of the lowest $T = 2$, $J^\pi = 0^+$ isobaric analog state in $^{52}$Co and its impact on the understanding of $\beta$-decay properties of $^{52}$Ni. Phys. Rev. Lett. **117**, 182503 (2016). https://doi.org/10.1103/PhysRevLett.117.182503
150. P. Zhang, X. Xu et al., High-precision $Q_{EC}$ values of superallowed $0^+ \rightarrow 0^+$ $\beta$-emitters $^{46}$Cr, $^{50}$Fe and $^{54}$Ni. Phys. Lett. B **767**, 20–24 (2017). https://doi.org/10.1016/j.physletb.2017.01.039
151. C.Y. Fu, Y.H. Zhang, X.H. Zhou et al., Masses of the $T_z = -3/2$ nuclei $^{27}$P and $^{29}$S. Phys. Rev. C **98**, 014315 (2018). https://doi.org/10.1103/PhysRevC.98.014315
152. Y.M. Xing, K.A. Li, Y.H. Zhang et al., Mass measurements of neutron-deficient Y, Zr, and Nb isotopes and their impact on rp and $\nu$p nucleosynthesis processes. Phys. Lett. B **781**, 358–363 (2018). https://doi.org/10.1016/j.physletb.2018.04.009
153. Y.H. Zhang, P. Zhang, X.H. Zhou et al., Isochronous mass measurements of $T_z = -1$ $fp$-shell nuclei from projectile fragmentation of $^{58}$Ni. Phys. Rev. C **98**, 014319 (2018). https://doi.org/10.1103/PhysRevC.98.014319
154. X. Xu, M. Wang, K. Blaum et al., Masses of neutron-rich $^{52-54}$Sc and $^{54,56}$Ti nuclides: The $N = 32$ subshell closure in scandium. Phys. Rev. C **99**, 064303 (2019). https://doi.org/10.1103/PhysRevC.99.064303
155. X. Xu, J.H. Liu, C.X. Yuan et al., Masses of ground and isomeric states of $^{101}$In and configuration-dependent shell evolution in odd-$A$ indium isotopes. Phys. Rev. C **100**, 051303 (2019). https://doi.org/10.1103/PhysRevC.100.051303
156. C.Y. Fu, Y.H. Zhang, M. Wang et al., Mass measurements for the $T_z = -2$ $fp$-shell nuclei $^{40}$Ti,$^{44}$ Cr, $^{46}$Mn, $^{48}$Fe, $^{50}$Co, and $^{52}$Ni. Phys. Rev. C **102**, 054311 (2020). https://doi.org/10.1103/PhysRevC.102.054311
157. Y.M. Xing, C.X. Yuan, M. Wang et al., Isochronous mass measurements of neutron-deficient nuclei from $^{112}$Sn projectile fragmentation. Phys. Rev. C **107**, 014304 (2023). https://doi.org/10.1103/PhysRevC.107.014304
158. M.-Z. Sun, X.-H. Zhou, M. Wang, Y.-H. Zhang, Y.A. Litvinov, Precision mass measurements of short-lived nuclides at HIRFL-CSR in Lanzhou. Front. Phys. **13**, 132112 (2018). https://doi.org/10.1007/s11467-018-0844-5
159. H. Geissel, Y.A. Litvinov, Precision experiments with relativistic exotic nuclei at GSI. J. Phys. G **31**, S1779–S1783 (2005). https://doi.org/10.1088/0954-3899/31/10/072
160. H. Geissel, R. Knöbel, Y.A. Litvinov et al., A new experimental approach for isochronous mass measurements of short-lived exotic nuclei with the FRS-ESR facility. Hyperf. Int. **173**, 49–54 (2006). https://doi.org/10.1007/s10751-007-9541-4
161. R. Knöbel, M. Diwisch, H. Geissel et al., New results from isochronous mass measurements of neutron-rich uranium fission fragments with the FRS-ESR-facility at GSI. Eur. Phys. J. A **52**, 138 (2016). https://doi.org/10.1140/epja/i2016-16138-6

162. R. Knöbel, M. Diwisch, F. Bosch et al., First direct mass measurements of stored neutron-rich $^{129,130,131}$Cd isotopes with FRS-ESR. Phys. Lett. B **754**, 288–293 (2016). https://doi.org/10.1016/j.physletb.2016.01.039
163. X.-L. Yan, R.-J. Chen, M. Wang et al., Characterization of a double Time-Of-Flight detector system for accurate velocity measurement in a storage ring using laser beams. Nucl. Instr. Meth. A **931**, 52–59 (2019). https://doi.org/10.1016/j.nima.2019.03.058
164. X. Xu, M. Wang, P. Shuai et al., A data analysis method for isochronous mass spectrometry using two time-of-flight detectors at CSRe. Chin. Phys. C **39**, 106201 (2015). https://doi.org/10.1088/1674-1137/39/10/106201
165. X. Zhou, M. Zhang, M. Wang et al., In-ring velocity measurement for isochronous mass spectrometry. Phys. Rev. Accel. Beams **24**, 042802 (2021). https://doi.org/10.1103/PhysRevAccelBeams.24.042802
166. M. Wang, M. Zhang, X. Zhou et al., B$\rho$-defined isochronous mass spectrometry: An approach for high-precision mass measurements of short-lived nuclei. Phys. Rev. C **106**, 051301 (2022). https://doi.org/10.1103/PhysRevC.106.L051301
167. M. Wang, et al. Mass measurements of upper $fp$-shell $N = Z-2$ and $N = Z - 1$ nuclei: the impact of three-nucleon forces on proton-neutron pairing correlations along $N = Z$ line. Phys. Rev. Lett., in print (2023)
168. M. Zhang, X. Zhou, M. Wang et al., B$\rho$-defined isochronous mass spectrometry and mass measurements of $^{58}$Ni fragments. Eur. Phys. J. A **59**, 27 (2023). https://doi.org/10.1140/epja/s10050-023-00928-6
169. X. Zhou, M. Wang, Y. H. Zhang, et al., Mass measurements show slowdown of rapid proton capture process at waiting-point nucleus $^{64}$Ge, Nat. Phys. (2023). https://doi.org/10.1038/s41567-023-02034-2 023-02034-2
170. National Nuclear Data Center. https://www.nndc.bnl.gov
171. H. Geissel, Y.A. Litvinov, F. Attallah et al., New results with stored exotic nuclei at relativistic energies. Nucl. Phys. A **746**, 150–155 (2004). https://doi.org/10.1016/j.nuclphysa.2004.09.030
172. F.G. Kondev, M. Wang, W.J. Huang, S. Naimi, G. Audi, The NUBASE2020 evaluation of nuclear physics properties. Chin. Phys. C **45**, 030001 (2021). https://doi.org/10.1088/1674-1137/abddae
173. F.C. Ozturk, B. Akkus, D. Atanasov et al., New test of modulated electron capture decay of hydrogen-like $^{142}$Pm ions: Precision measurement of purely exponential decay. Phys. Lett. B **797**, 134800 (2019). https://doi.org/10.1016/j.physletb.2019.134800
174. F. Bosch, Y.A. Litvinov, Mass and lifetime measurements at the experimental storage ring of GSI. Int. J. Mass Spectrom. **349–350**, 151–161 (2013). https://doi.org/10.1016/j.ijms.2013.04.025
175. B. Sun, R. Knobel, N. Kuzminchuk et al., A new resonator Schottky pick-up for short-lived nuclear investigations. GSI Sci. Rep. **2011**, 163 (2012)
176. X.L. Tu, X.C. Chen, J.T. Zhang et al., First application of combined isochronous and Schottky mass spectrometry: Half-lives of fully ionized $^{49}$Cr$^{24+}$ and $^{53}$Fe$^{26+}$ atoms. Phys. Rev. C **97**, 014321 (2018). https://doi.org/10.1103/PhysRevC.97.014321
177. W. Korten, et al., Search for the nuclear two-photon decay in swift fully-stripped heavy ions. Proposal for GSI Program Advisory Committee (2020)
178. P.M. Walker, Y.A. Litvinov, H. Geissel, The ILIMA project at FAIR. Int. J. Mass Spectrom. **349–350**, 247–254 (2013). https://doi.org/10.1016/j.ijms.2013.04.007
179. O. Klepper, F. Bosch, H.W. Daues et al., First steps towards radioactive beams in the experimental storage ring at GSI. Nucl. Instr. Meth. B **70**, 427–433 (1992). https://doi.org/10.1016/0168-583X(92)95960-Y
180. O. Klepper, C. Kozhuharov, Particle detectors for beam diagnosis and for experiments with stable and radioactive ions in the storage-cooler ring ESR. Nucl. Instr. Meth. B **204**, 553–556 (2003). https://doi.org/10.1016/S0168-583X(02)02131-6
181. M.A. Najafi, I. Dillmann, F. Bosch et al., CsI-silicon particle detector for heavy ions orbiting in storage rings (CsISiPHOS). Nucl. Instr. Meth. A **836**, 1–6 (2016). https://doi.org/10.1016/j.nima.2016.08.040
182. N. Petridis, A. Kalinin, U. Popp et al., Energy loss and cooling of relativistic highly charged uranium ions interacting with an internal hydrogen droplet target beam. Nucl. Instr. Meth. A **656**, 1–4 (2011). https://doi.org/10.1016/j.nima.2011.07.035
183. N. Petridis, R.E. Grisenti, Y.A. Litvinov, T. Stöhlker, Prototype internal target design for storage ring experiments. Phys. Scripta **T166**, 014051 (2015). https://doi.org/10.1088/0031-8949/2015/T166/014051
184. J. Eichler, T. Stöhlker, Radiative electron capture in relativistic ion-atom collisions and the photoelectric effect in hydrogen-like high-Z systems. Phys. Rep. **439**, 1–99 (2007). https://doi.org/10.1016/j.physrep.2006.11.003
185. V.P. Shevelko, Y.A. Litvinov, T. Stöhlker, I.Y. Tolstikhina, Lifetimes of relativistic heavy-ion beams in the high energy storage ring of FAIR. Nucl. Instr. Meth. B **421**, 45–49 (2018). https://doi.org/10.1016/j.nimb.2018.02.012
186. H. Irnich, H. Geissel, F. Nolden et al., Half-life measurements of bare, mass-resolved isomers in a storage-cooler ring. Phys. Rev. Lett. **75**, 4182–4185 (1995). https://doi.org/10.1103/PhysRevLett.75.4182
187. R. Daudel, M. Jean, M. Lecoin, Sur la possibilité d'existence d'un type particulier de radioactivité phénomène de créatione. J. Phys. Radium **8**, 238–243 (1947). https://doi.org/10.1051/jphysrad:0194700808023800
188. J.N. Bahcall, Theory of bound-state beta decay. Phys. Rev. **124**, 495–499 (1961). https://doi.org/10.1103/PhysRev.124.495
189. W. Bambynek, H. Behrens, M.H. Chen et al., Orbital electron capture by the nucleus. Rev. Mod. Phys. **49**, 77–221 (1977). https://doi.org/10.1103/RevModPhys.49.77
190. M. Jung, F. Bosch, K. Beckert et al., First observation of bound-state $\beta^-$ decay. Phys. Rev. Lett. **69**, 2164–2167 (1992). https://doi.org/10.1103/PhysRevLett.69.2164
191. F. Bosch, T. Faestermann, J. Friese et al., Observation of Bound-State $\beta^-$ Decay of Fully Ionized $^{187}$Re: $^{187}$Re—$^{187}$Os Cosmochronometry. Phys. Rev. Lett. **77**, 5190–5193 (1996). https://doi.org/10.1103/PhysRevLett.77.5190
192. K. Takahashi, The $^{187}$Re-$^{187}$Os cosmochronometry-the latest developments. AIP Conf. Proc. **425**, 616–625 (1998). https://doi.org/10.1063/1.55179
193. T. Ohtsubo, F. Bosch, H. Geissel et al., Simultaneous measurement of $\beta^-$ decay to bound and continuum electron states. Phys. Rev. Lett. **95**, 052501 (2005). https://doi.org/10.1103/PhysRevLett.95.052501
194. J. Kurcewicz, F. Bosch, H. Geissel et al., Studies of two-body $\beta$-decays at the FRS-ESR facility. Acta Phys. Polon. B **41**, 525–536 (2010)
195. M.K. Pavicevic, Lorandite from Allchar—A low energy solar neutrino dosimeter. Nucl. Instr. Meth. A **271**, 287–296 (1988). https://doi.org/10.1016/0168-9002(88)90171-4
196. B.S. Meyer, D.D. Clayton, Short-lived radioactivities and the birth of the Sun. Space Sci. Rev. **92**, 133–152 (2000). https://doi.org/10.1023/A:1005282825778
197. M.S. Freedman, C.M. Stevens, E.P. Horwitz et al., Solar neutrinos: proposal for a new test. Science **193**, 1117–1119 (1976). https://doi.org/10.1126/science.193.4258.1117
198. W. Henning, W. Kutschera, H. Ernst et al., The $^{205}$Tl experiment. AIP Conf. Proc. **126**, 203–211 (1985). https://doi.org/10.1063/1.35150
199. M.K. Pavicevic, G. Amthauer, V. Cvetkovic et al., Lorandite from Allchar as geochemical detector for pp-solar neutrinos. Nucl.

Instr. Meth. A **895**, 62–73 (2018). https://doi.org/10.1016/j.nima.2018.03.039
200. J. Kostensalo, J. Suhonen, K. Zuber, Calculated solar-neutrino capture rate for a radiochemical $^{205}$Tl-based solar-neutrino detector. Phys. Rev. C **101**, 031302 (2020). https://doi.org/10.1103/PhysRevC.101.031302
201. S. Liu, C. Gao, C. Xu, Investigation of bound state $\beta^-$ decay half-lives of bare atoms. Phys. Rev. C **104**, 024304 (2021). https://doi.org/10.1103/PhysRevC.104.024304
202. Y.A. Litvinov, F. Bosch, H. Geissel et al., Measurement of the $\beta^+$ and orbital electron-capture decay rates in fully ionized, hydrogenlike, and heliumlike $^{140}$Pr ions. Phys. Rev. Lett. **99**, 262501 (2007). https://doi.org/10.1103/PhysRevLett.99.262501
203. N. Winckler, H. Geissel, Y.A. Litvinov et al., Orbital electron capture decay of hydrogen- and helium-like $^{142}$Pm ions. Phys. Lett. B **679**, 36–40 (2009). https://doi.org/10.1016/j.physletb.2009.07.019
204. D.R. Atanasov, N. Winckler, D. Balabanski et al., Half-life measurements of stored fully ionized and hydrogen-like $^{122}$I ions. Eur. Phys. J. A **48**, 22 (2012). https://doi.org/10.1140/epja/i2012-12022-9
205. Z. Patyk, J. Kurcewicz, F. Bosch, H. Geissel, Y.A. Litvinov, M. Pfützner, Orbital electron capture decay of hydrogen- and helium-like ions. Phys. Rev. C **77**, 014306 (2008). https://doi.org/10.1103/PhysRevC.77.014306
206. J. Kurcewicz, Y.A. Litvinov, F. Bosch et al., Orbital electron capture and $\beta^+$ decay of H-Like $^{140}$Pr ions. Acta Phys. Polon. B **39**, 501–506 (2008)
207. K. Siegień-Iwaniuk, N. Winckler, F. Bosch, H. Geissel, Y.A. Litvinov, Z. Patyk, Orbital electron capture of hydrogen- and helium-like ions. Phys. Rev. C **84**, 014301 (2011). https://doi.org/10.1103/PhysRevC.84.014301
208. A.N. Ivanov, M. Faber, R. Reda, P. Kienle, Weak decays of H-like $^{140}$Pr$^{58+}$ and He-like $^{140}$Pr$^{57+}$ ions. Phys. Rev. C **78**, 025503 (2008). https://doi.org/10.1103/PhysRevC.78.025503
209. H. Primakoff, Theory of muon capture. Rev. Mod. Phys. **31**, 802–822 (1959). https://doi.org/10.1103/RevModPhys.31.802
210. Y.A. Litvinov, F. Bosch, N. Winckler et al., Observation of non-exponential orbital electron capture decays of hydrogen-like $^{140}$Pr and $^{142}$Pm ions. Phys. Lett. B **664**, 162–168 (2008). https://doi.org/10.1016/j.physletb.2008.04.062
211. F. Bosch, Y.A. Litvinov, Observation of non-exponential orbital electron-capture decay of stored hydrogen-like ions. Prog. Part. Nucl. Phys. **64**, 435–438 (2010). https://doi.org/10.1016/j.ppnp.2009.12.069
212. T. Faestermann, Lifetime measurements of nuclei in few-electron ions. Phys. Scripta **T166**, 014003 (2015). https://doi.org/10.1088/0031-8949/2015/t166/014003
213. P. Walker, G. Dracoulis, Energy traps in atomic nuclei. Nature **399**, 35–40 (1999). https://doi.org/10.1038/19911
214. P.M. Walker, G.D. Dracoulis, Exotic isomers in deformed atomic nuclei. Hyperf. Int. **135**, 83–107 (2001). https://doi.org/10.1023/A:1013915200556
215. P. Walker, Z. Podolyák, 100 years of nuclear isomers-then and now. Phys. Scripta **95**, 044004 (2020). https://doi.org/10.1088/1402-4896/ab635d
216. W.R. Phillips, I. Ahmad, D.W. Banes et al., Charge-state dependence of nuclear lifetimes. Phys. Rev. Lett. **62**, 1025–1028 (1989). https://doi.org/10.1103/PhysRevLett.62.1025
217. W.R. Phillips, J. Copnell, D.W. Banes et al., Electron-nucleus interactions in few-electron Fe ions. Phys. Rev. A **47**, 3682–3691 (1993). https://doi.org/10.1103/PhysRevA.47.3682
218. F. Attallah, M. Aiche, J.F. Chemin et al., Ionic charge dependence of the internal conversion coefficient and nuclear lifetime of the first excited state in $^{125}$Te. Phys. Rev. C **55**, 1665–1675 (1997). https://doi.org/10.1103/PhysRevC.55.1665
219. M.R. Harston, T. Carreyre, J.F. Chemin, F. Karpeshin, M.B. Trzhaskovskaya, Internal conversion to bound final states in $^{125}$Te. Nucl. Phys. A **676**, 143–154 (2000). https://doi.org/10.1016/S0375-9474(00)00196-2
220. Y.A. Litvinov, F. Attallah, K. Beckert et al., Observation of a dramatic hindrance of the nuclear decay of isomeric states for fully ionized atoms. Phys. Lett. B **573**, 80–85 (2003). https://doi.org/10.1016/j.physletb.2003.08.077
221. M.W. Reed, I.J. Cullen, P.M. Walker et al., Discovery of highly excited long-lived isomers in neutron-rich hafnium and tantalum isotopes through direct mass measurements. Phys. Rev. Lett. **105**, 172501 (2010). https://doi.org/10.1103/PhysRevLett.105.172501
222. M.W. Reed, P.M. Walker, I.J. Cullen et al., Long-lived isomers in neutron-rich $Z = 72 - 76$ nuclides. Phys. Rev. C **86**, 054321 (2012). https://doi.org/10.1103/PhysRevC.86.054321
223. M.W. Reed, P.M. Walker, I.J. Cullen et al., Technique for resolving low-lying isomers in the experimental storage ring (esr) and the occurrence of an isomeric state in$^{192}$Re. J. Phys. Conf. Series **381**, 012058 (2012). https://doi.org/10.1088/1742-6596/381/1/012058
224. P.M. Walker, Y. Hirayama, G.J. Lane et al., Properties of $^{187}$Ta revealed through isomeric decay. Phys. Rev. Lett. **125**, 192505 (2020). https://doi.org/10.1103/PhysRevLett.125.192505
225. Y.X. Watanabe, P.M. Walker, Y. Hirayama et al., First direct observation of isomeric decay in neutron-rich odd-odd $^{186}$Ta. Phys. Rev. C **104**, 024330 (2021). https://doi.org/10.1103/PhysRevC.104.024330
226. M. Mukai, Y. Hirayama, Y.X. Watanabe et al., Ground-state $\beta$-decay spectroscopy of $^{187}$Ta. Phys. Rev. C **105**, 034331 (2022). https://doi.org/10.1103/PhysRevC.105.034331
227. B. Sun, F. Bosch, D. Boutin et al., Precise measurement of nuclear isomers in the storage ring at GSI. Nucl. Phys. A **834**, 476–478 (2010). https://doi.org/10.1016/j.nuclphysa.2010.01.069
228. B. Sun, R. Knöbel, H. Geissel et al., Direct measurement of the 4.6 MeV isomer in stored bare $^{133}$Sb ions. Phys. Lett. B **688**, 294–297 (2010). https://doi.org/10.1016/j.physletb.2010.04.020
229. Q. Zeng, M. Wang, X.H. Zhou et al., Half-life measurement of short-lived $^{94m}_{44}$Ru$^{44+}$ using isochronous mass spectrometry. Phys. Rev. C **96**, 031303 (2017). https://doi.org/10.1103/PhysRevC.96.031303
230. M.S. Sanjari, X. Chen, P. Hülsmann et al., Conceptual design of elliptical cavities for intensity and position sensitive beam measurements in storage rings. Phys. Scripta **T166**, 014060 (2015). https://doi.org/10.1088/0031-8949/2015/T166/014060
231. X. Chen, M.S. Sanjari, P. Hülsmann et al., Intensity-sensitive and position-resolving cavity for heavy-ion storage rings. Nucl. Instr. Meth. A **826**, 39–47 (2016). https://doi.org/10.1016/j.nima.2016.04.056
232. D. Dmytriiev, M.S. Sanjari, Y.A. Litvinov, T. Stöhlker, Position sensitive resonant Schottky cavities for heavy ion storage rings. Nucl. Instr. Meth. B **463**, 320–323 (2020). https://doi.org/10.1016/j.nimb.2019.04.074
233. I.N. Borzov, Beta-decay rates. Nucl. Phys. A **777**, 645–675 (2006). https://doi.org/10.1016/j.nuclphysa.2005.05.147
234. Z. Podolyák, Competition between allowed and first-forbidden beta decays and the r-process. EPJ Web Conf. **260**, 03005 (2022). https://doi.org/10.1051/epjconf/202226003005
235. I. Dillmann, Y.A. Litvinov, r-Process nucleosynthesis: Present status and future experiments at the FRS and ESR. Prog. Part. Nucl. Phys. **66**, 358–362 (2011). https://doi.org/10.1016/j.ppnp.2011.01.034
236. A. Evdokimov, I. Dillmann, M. Marta et al., An alternative approach to measure $\beta$-delayed neutron emission. Proc. Sci. **12**, 115 (2013). https://doi.org/10.22323/1.146.0115

237. C. Griffin, et al., Symbiotic measurement of masses, half-lives, and neutron branching ratios of $^{137,138}$I at the ESR. Proposal for GSI Program Advisory Committee (2022)
238. I. Mukha, Private communications (2014-2020)
239. Z. Patyk, H. Geissel, Y.A. Litvinov, A. Musumarra, C. Nociforo, $\alpha$-decay half-lives for neutral atoms and bare nuclei. Phys. Rev. C **78**, 054317 (2008). https://doi.org/10.1103/PhysRevC.78.054317
240. A. Musumarra, F. Farinon, C. Nociforo et al., Electron screening effects on $\alpha$-decay. AIP Conf. Proc. **1165**, 415–418 (2009). https://doi.org/10.1063/1.3232139
241. C. Nociforo, F. Farinon, A. Musumarra et al., Measurements of $\alpha$-decay half-lives at GSI. Phys. Scripta **T150**, 014028 (2012). https://doi.org/10.1088/0031-8949/2012/t150/014028
242. F.F. Karpeshin, M.B. Trzhaskovskaya, Experimental aspects of the adiabatic approach in estimating the effect of electron screening on alpha decay. Phys. At. Nucl. **78**, 993–1000 (2015). https://doi.org/10.1134/S1063778815090082
243. Y.A. Litvinov, Mass and lifetime measurements at the present ESR facility. Int. J. Mod. Phys. E **18**, 323–334 (2009). https://doi.org/10.1142/S0218301309012355
244. P. Seelig, S. Borneis, A. Dax et al., Ground state hyperfine splitting of hydrogenlike $^{207}$Pb$^{81+}$ by laser excitation of a bunched ion beam in the GSI experimental storage ring. Phys. Rev. Lett. **81**, 4824–4827 (1998). https://doi.org/10.1103/PhysRevLett.81.4824
245. Y.A. Litvinov, Mass and half-life measurements of stored exotic nuclei at the FRS-ESR facility. Nucl. Phys. A **805**, 260–269 (2008). https://doi.org/10.1016/j.nuclphysa.2008.02.254
246. M. Grieser, Y.A. Litvinov, R. Raabe et al., Storage ring at HIE-ISOLDE. Eur. Phys. J. Special Topics **207**, 1–117 (2012). https://doi.org/10.1140/epjst/e2012-01599-9
247. R.S. Sidhu, et al., Influence of hyperfine interaction on the nuclear electron capture decay in $^{111}$Sn. Proposal for GSI Program Advisory Committee (2022)
248. K. Siegień-Iwaniuk, Z. Patyk, Nuclear electron capture in Li-like ions. Phys. Rev. C **84**, 064309 (2011). https://doi.org/10.1103/PhysRevC.84.064309
249. W. Korten, et al., Nuclear two-photon decay and bound-state pair conversion. Proposal for GSI Program Advisory Committee (2022)
250. F. Bosch, S. Hagmann, P.-M. Hillenbrand et al., Search for bound-state electron+positron pair decay. EPJ Web Conf. **123**, 04003 (2016). https://doi.org/10.1051/epjconf/201612304003
251. G.C. Rodrigues, P. Indelicato, J.P. Santos, P. Patte, F. Parente, Systematic calculation of total atomic energies of ground state configurations. At. Data Nucl. Data Tab. **86**, 117–233 (2004). https://doi.org/10.1016/j.adt.2003.11.005
252. C.J. Chiara, J.J. Carroll, M.P. Carpenter et al., Isomer depletion as experimental evidence of nuclear excitation by electron capture. Nature **554**, 216–218 (2018). https://doi.org/10.1038/nature25483
253. Y. Wu, C.H. Keitel, A. Pálffy, $^{93m}$Mo isomer depletion via beam-based nuclear excitation by electron capture. Phys. Rev. Lett. **122**, 212501 (2019). https://doi.org/10.1103/PhysRevLett.122.212501
254. J. Rzadkiewicz, M. Polasik, K. Słabkowska, L. Syrocki, J.J. Carroll, C.J. Chiara, Novel approach to $^{93m}$Mo isomer depletion: Nuclear excitation by electron capture in resonant transfer process. Phys. Rev. Lett. **127**, 042501 (2021). https://doi.org/10.1103/PhysRevLett.127.042501
255. S. Guo, B. Ding, X.H. Zhou et al., Probing $^{93m}$Mo isomer depletion with an isomer beam. Phys. Rev. Lett. **128**, 242502 (2022). https://doi.org/10.1103/PhysRevLett.128.242502
256. A. Zylstra, et al., Heavy ion storage ring experiments of nuclear excitation by electron capture (NEEC). Proposal for GSI Program Advisory Committee (2022)
257. Y.A. Litvinov, et al., Nuclear excitation by electron capture (NEEC) measurements using the ESR electron cooler as a target for free electrons. Proposal for GSI Program Advisory Committee (2020)
258. B. Seiferle, L. von der Wense, P.V. Bilous et al., Energy of the $^{229}$Th nuclear clock transition. Nature **573**, 243–246 (2019). https://doi.org/10.1038/s41586-019-1533-4
259. P.G. Thirolf, B. Seiferle, L. von der Wense, The 229-thorium isomer: doorway to the road from the atomic clock to the nuclear clock. J. Phys. B **52**, 203001 (2019). https://doi.org/10.1088/1361-6455/ab29b8
260. Webpage of the European Thorium Nuclear Clock project (2023). https://thoriumclock.eu/
261. V.M. Shabaev, D.A. Glazov, A.M. Ryzhkov et al., Ground-state $g$ factor of highly charged $^{229}$Th ions: An access to the m1 transition probability between the isomeric and ground nuclear states. Phys. Rev. Lett. **128**, 043001 (2022). https://doi.org/10.1103/PhysRevLett.128.043001
262. C. Brandau, et al., Laser excitation of the $^{229}$Th nucleus using nuclear hyperfine mixing. Proposal for GSI Program Advisory Committee (2020)
263. C. Brandau, et al., Follow-Up E142: laser excitation of the $^{229}$Th nucleus using nuclear hyperfine mixing. Proposal for GSI Program Advisory Committee (2022)
264. J. Jin, et al., Excitation and probing of low-energy nuclear states at high-energy storage rings. Phys. Rev. Res., in print (2023)
265. M. Durante, P. Indelicato, B. Jonson et al., All the fun of the FAIR: fundamental physics at the facility for antiproton and ion research. Phys. Scripta **94**, 033001 (2019). https://doi.org/10.1088/1402-4896/aaf93f
266. A. Dolinskii, F. Nolden, M. Steck, Lattice considerations for the collector and the accumulator ring of the FAIR project. In: Proc., Workshop on Beam Cooling and Related Topics, pp. 106–109 (2007). http://accelconf.web.cern.ch/AccelConf/cl07/PAPERS/TUA2C08.PDF
267. H. Geissel, H. Weick, M. Winkler et al., The Super-FRS project at GSI. Nucl. Instr. Meth. B **204**, 71–85 (2003). https://doi.org/10.1016/S0168-583X(02)01893-1
268. R. Maier, The high-energy storage ring (HESR). In: Proc., 2011 Particle Accelerator Conference, p. 2014 (2011). http://accelconf.web.cern.ch/accelconf/pac2011/papers/thocn2.pdf
269. T. Stöhlker, Y.A. Litvinov, V. Bagnoud et al., SPARC experiments at the high-energy storage ring. Phys. Scr. **T156**, 014085 (2013). https://doi.org/10.1088/0031-8949/2013/T156/014085
270. J.C. Yang, J.W. Xia, G.Q. Xiao et al., High intensity heavy ion accelerator facility (HIAF) in China. Nucl. Instr. Meth. B **317**, 263–265 (2013). https://doi.org/10.1016/j.nimb.2013.08.046
271. B. Wu, J.C. Yang, J.W. Xia et al., The design of the Spectrometer Ring at the HIAF. Nucl. Instr. Meth. A **881**, 27–35 (2018). https://doi.org/10.1016/j.nima.2017.08.017
272. X. Zhou, Physics opportunities at the new facility HIAF. Nucl. Phys. Rev. **35**, 339 (2018). https://doi.org/10.11804/NuclPhysRev.35.04.339
273. X. Ma, W.Q. Wen, S.F. Zhang et al., HIAF: New opportunities for atomic physics with highly charged heavy ions. Nucl. Instr. Meth. B **408**, 169–173 (2017). https://doi.org/10.1016/j.nimb.2017.03.129
274. X. Ma, W.Q. Wen, S.F. Zhan et al., Atomic physics research at HIAF and future perspective. J. Phys. Conf. Series **1412**, 232005 (2020). https://doi.org/10.1088/1742-6596/1412/23/232005
275. Opportunities with Neutron Induced Reaction Measurements (Santa Fe, 24-25 November 2020). https://indico.cern.ch/event/928894/

276. North American Storage Rings & Neutron Captures Workshop (TRIUMF, 28-30 June 2021). https://meetings.triumf.ca/event/235/
277. R. Reifarth, Y.A. Litvinov, Measurements of neutron-induced reactions in inverse kinematics. Phys. Rev. ST Accel. Beams **17**, 014701 (2014). https://doi.org/10.1103/PhysRevSTAB.17.014701
278. R. Reifarth, K. Göbel, T. Heftrich et al., Spallation-based neutron target for direct studies of neutron-induced reactions in inverse kinematics. Phys. Rev. Accel. Beams **20**, 044701 (2017). https://doi.org/10.1103/PhysRevAccelBeams.20.044701
279. L.V. Grigorenko, B.Y. Sharkov, A.S. Fomichev et al., Scientific program of DERICA - prospective accelerator and storage ring facility for radioactive ion beam research. Phys. Usp. **62**, 675–690 (2019). https://doi.org/10.3367/ufne.2018.07.038387
280. B. Sun, Y.A. Litvinov, P.M. Walker et al., Discovery of a new long-lived isomeric state in $^{125}$Ce. Eur. Phys. J. A **31**, 393–394 (2007). https://doi.org/10.1140/epja/i2006-10252-0
281. F. Attallah, M. Hausmann, Y.A. Litvinov et al., Mass and lifetime measurements at the storage ring ESR. Nucl. Phys. A **701**, 561–564 (2002). https://doi.org/10.1016/S0375-9474(01)01644-X
282. A. Akber, M.W. Reed, P.M. Walker et al., Increased isomeric lifetime of hydrogen-like $^{192m}$Os. Phys. Rev. C **91**, 031301 (2015). https://doi.org/10.1103/PhysRevC.91.031301
283. L. Chen, W.R. Plass, H. Geissel et al., Discovery and investigation of heavy neutron-rich isotopes with time-resolved Schottky spectrometry in the element range from thallium to actinium. Phys. Lett. B **691**, 234–237 (2010). https://doi.org/10.1016/j.physletb.2010.05.078
284. L. Chen, P.M. Walker, H. Geissel et al., Direct observation of long-lived isomers in $^{212}$Bi. Phys. Rev. Lett. **110**, 122502 (2013). https://doi.org/10.1103/PhysRevLett.110.122502
285. L.X. Chen, Investigation of stored neutron-rich nuclides in the element range of Pt–U with the FRS-ESR facility at 360–400 MeV/u. PhD thesis, Univerisity of Giessen (2008)